THE ASTRONOMICAL JOURNAL VOLUME 109, NUMBER 3 MARCH 1995

POLAR RING SPIRAL GALAXY NGC 660

W. VAN DRIEL

Kiso Observatory, Institute of Astronomy, The University of Tokyo, Mitake-mura, Kiso-gun, Nagano-ken 397-01, Japan and Astronomical Institute "Anton Pannekoek," University of Amsterdam, Kruislaan 403, 1098 SJ Amsterdam, The Netherlands and Nançay Radio Observatory, USN, Observatoire de Paris-Meudon, 92195 Meudon Cedex Principal, France
Electronic mail: vandriel@obspm.fr

F. COMBES AND F. CASOLI

DEMIRM, Observatoire de Paris, 61 Ave de l'Observatoire, 75014 Paris, France
Electronic mail: bottaro@obspm.fr, casoli@obspm.fr

M. GERIN

Radioastronomie Millimétrique, Laboratoire de Physique de l'Ecole Normale Supérieure, 24 Rue Lhomond, 75231 Paris, France
Electronic mail: gerin@ensapa.ens.fr

N. NAKAI AND T. MIYAJI

Nobeyama Radio Observatory, Nobeyama, Minamisaku, Nagano-ken 384-13, Japan
Electronic mail: nakai@nro.nao.ac.jp, miyaji@mb2044.nro.nao.ac.jp

M. HAMABE, Y. SOFUE, T. ICHIKAWA, AND S. YOSHIDA

Kiso Observatory, Institute of Astronomy, The University of Tokyo, Mitake-mura, Kiso-gun, Nagano-ken 397-01, Japan
Electronic mail: mhamabe@mtk.ioa.s.u-tokyo.ac.jp, sofue@mtk.ioa.s.u-tokyo.ac.jp, ichikawa@kiso.ioa.s.u-tokyo.ac.jp, yoshida@kiso.ioa.s.u-tokyo.ac.jp

Y. KOBAYASHI, F. GENG, AND T. MINEZAKI

National Astronomical Observatory, 2-21-1 Osawa, Mitaka, Tokyo 181, Japan and Department of Astronomy, School of Science, The University of Tokyo, 2-11-16 Yayoi, Bunkyo-ku, Tokyo 113, Japan
Electronic mail: okabaya@c1.mtk.nao.ac.jp, ofang@c1.mtk.nao.ac.jp, omineza@c1.mtk.nao.ac.jp

N. ARIMOTO AND T. KODAMA

Institute of Astronomy, The University of Tokyo, 2-21-1 Osawa, Mitaka, Tokyo 181, Japan
Electronic mail: arimoto@mtk.ioa.s.u-tokyo.ac.jp, kodama@cl.mtk.nao.ac.jp

P. GOUDFROOIJ

European Southern Observatory, Karl-Schwarzschildstrasse 2, D-85748 Garching bei München, Germany and Astronomical Institute "Anton Pannekoek," University of Amsterdam, Kruislaan 403, 1098 SJ Amsterdam, The Netherlands
Electronic mail: pgoudfro@eso.org

P. S. MULDER

Kapteyn Laboratory, Kapteyn Astronomical Institute, P. O. Box 800, 9700 AV Groningen, The Netherlands
Electronic mail: pieterm@astro.rug.nl

K. WAKAMATSU

Department of Physics, College of Technology, Gifu University, Yanagido, Gifu-ken 501-11, Japan
Electronic mail: waka@oph.info.gifu-u.ac.jp

K. YANAGISAWA

Department of Astronomy and Earth Sciences, Tokyo Gakugei University, Koganei, Tokyo 184, Japan
Electronic mail: byanagi@c1.mtk.nao.ac.jp

Received 1994 June 3; revised 1994 November 9

 0004-6256/95/109(3)/942/18/$0.90

ABSTRACT

NGC 660 is a unique, nearby, peculiar polar ring spiral LINER galaxy with two distinct morphological and kinematic components: a spiral disk, seen almost edge on ($i \sim 70°$), with a major axis position angle of 45° and a diameter of ~11 kpc ($D = 13$ Mpc, $H_0 = 75$ km s^{-1} Mpc^{-1}), and an outer polar ring (P.A. 170°) with a diameter of 31 kpc, inclined on average 55° with respect to the disk major axis. It was mapped in the 21 cm H I line with a resolution of 13″×60″ and in the CO(1–0) and CO(2–1) lines with a 12″–22″ beam. B, V, R, I, J, H, K'-band images, and a long-slit Hα spectrum along the disk major axis were obtained as well. It has been morphologically classified as SBa, but our data show it has the global characteristics of a later-type (Sc?), gas-rich disk. The disk and the polar ring both have an exponential luminosity profile, with scale lengths of 1.3 and 3.9 kpc, respectively. The polar ring is blue ($V-I \sim 1.0$), indicating a stellar population age of a few billion years, according to our stellar population synthesis model and the nucleus is red ($V-I \sim 1.8$). Hα images show H II regions throughout the polar ring. The near-infrared images show a boxy/X shape of the bulge and 1.4 kpc long linear features along the disk major axis on both sides of the bulge. The disk was detected in radio continuum at 21 cm. It has a compact 300 mJy nuclear source and an extended (7.5 kpc diameter) component of 80 mJy. The central source has a very high radio power for a spiral galaxy, while the disk has a normal radio power. The radio spectral index is −0.57, indicating an important contribution from thermal radiation. The H I line observations show absorption against the nuclear source, and both H I and CO line data show emission from the disk and the polar ring. The H I and CO data indicate a rather flat disk rotation curve, with a rotation velocity of ~150 km s^{-1}. From our Hα spectrum, taken close to the major axis, a steeper inner gradient and a considerably lower rotation velocity (~110 km s^{-1}) is derived in the outer parts than from that of Benvenuti *et al.* (1976), if one assumes the disk to be flat and in circular rotation. This probably indicates noncircular motions in the inner disk. Using a geometrical model it was found that the ring has a slightly rising rotation curve reaching 127 km s^{-1} at 18 kpc radius ($=1.15\,R_{25}$), implying an $\mathcal{M}_T/L_B^0$ ratio of $\sim 10 \mathcal{M}_\odot/L_{\odot,B}$ within this radius. The total H I and H_2 mass is about 5.4 and 3.7 10^9 $\mathcal{M}_\odot$, respectively. About 75% of the H I gas resides in the ring, and the disk has a gas content ($\mathcal{M}_{\mathrm{H\,I}}/L_B^0 = 0.3 \mathcal{M}_\odot/L_{\odot,B}$) of about an Sc-type spiral. Though the galaxy has a LINER-type spectrum, suggesting (like other indicators) intense massive star formation in the nucleus, and though it has a rather high far-infrared luminosity [$\log(L_{\mathrm{FIR}}/L_\odot) = 10.30$] as well as a high L_{FIR}/L_B^0 ratio (4.7), its overall star formation efficiency, $L_{\mathrm{FIR}}/\mathcal{M}_{\mathrm{H_2}} = 5.4 L_\odot/\mathcal{M}_\odot$, is comparable to that of normal spirals of similar L_{FIR}, and much lower than that of classical starburst galaxies. A mass model was made by fitting the luminosity profiles of the bulge, disk, and polar ring, as well as the rotation velocities in the disk, using a constant mass-to-light ratio, taking the gas mass into account. In order to fit the rotation velocities in the polar ring additional dark matter was required, however, with a dark-to-luminous mass ratio of 0.6 inside 18 kpc radius, if the halo is assumed to be spherical. The polar ring is quite massive, with a mass of about 75% of that of the disk, and it contains about 25% of the total estimated mass of the NGC 660 system. The considerable mass of the ring can explain its apparent stability through self-gravity. It was not possible to constrain the flattening of the dark halo, though, since the equatorial (disk) velocities at the radii of the polar ring are not known. In fact, this is true for all polar-ring systems, since two perpendicular streams of gas at the same radius do not form a stable situation. In the H I line the Irr? galaxy UGC 1195 was detected as well, at a projected distance of 82 kpc with a systemic velocity 74 km s^{-1} lower than NGC 660. It is gas-rich ($\mathcal{M}_{\mathrm{H\,I}}/L_B^0 = 0.4 \mathcal{M}_\odot/L_{\odot,B}$) with an H I distribution slightly larger than the optical outlines. It has a rather low rotation velocity of 56 km s^{-1}, implying $\mathcal{M}_T/L_B^0 \sim 2.6 \mathcal{M}_\odot/L_{\odot,B}$ within $R = 6.4$ kpc.

1. INTRODUCTION

NGC 660 is a unique, nearby, object among the rare class of polar ring galaxies, since it has a polar ring with an unusual morphology and a gas-rich inner disk with a nuclear LINER spectrum, while other objects of this class usually have a quiescent lenticular-type disk. It has two distinct morphological and kinematic components: a disk, viewed almost edge on, and an outer ring, inclined some 55° with respect to the major axis of the disk. Though not truly "polar" (i.e., perpendicular to the disk), it can still be regarded as such for all practical purposes, and we will therefore refer to it as a polar ring. The ring appears to be rather inclined, twisted, and warped, see also Whitmore *et al.* (1987) and Sec. 6. A nuclear starburst might be occurring in the disk, as indicated by its optical LINER and midinfrared spectrum, and a rather high far-infrared luminosity [$\log(L_{\mathrm{FIR}}/L_\odot) = 10.30$] and far-infrared/blue luminosity ratio (4.7). For a recent review on polar ring galaxies, see Combes (1994).

The present paper is our second on the intriguing NGC 660 system. In a previous paper (Combes *et al.* 1992, hereafter referred to as Paper I) we presented the detection of CO(1–0) line emission in the polar ring, and a three-dimensional geometrical model of the system, fitting the morphology and kinematics of the system, derived from optical and H I line data; our model is similar to the one derived

by Arnaboldi & Galletta (1993). In this paper we present new multiwavelength observations, as well as a detailed mass model of the galaxy. Short presentations of our results are given in van Driel (1995) and van Driel *et al.* (1994).

We were interested in studying the kinematics and morphology of NGC 660 at different wavelengths, since the kinematics of the disk and the polar ring could in principle be used to give insight in the three-dimensional shape of the mass distribution. In most polar ring galaxies the disk rotation can be studied using stellar absorption lines only, but gas-rich NGC 660 has the advantage that we can use accurate emission line velocities in both polar ring and disk, which do not require estimated corrections for asymmetric drift either. Also, a combination of high resolution CO(1–0) and CO(2–1) line observations allows us to investigate the molecular gas excitation in this nearby active galaxy.

We adopted a distance of 13.0 Mpc for both NGC 660 and nearby UGC 1195 (see Sec. 2), based on their H I redshifts (846 and 772 km s^{-1}, respectively) and H_0=75 km s^{-1} Mpc^{-1}, following de Vaucouleurs *et al.* (1976) without applying a correction for the infall towards the Virgo Cluster. This distance is in close agreement with the 12.8 Mpc derived using the H I line Tully–Fisher relation (Fukugita *et al.* 1991). Note that all radial velocities in this paper are heliocentric and calculated according to the conventional optical definition ($V=c\Delta\lambda/\lambda_0$), all coordinates are given for equinox (1950.0), and the solar magnitudes used are from Allen (1973)—$L_\odot$ denotes the solar bolometric luminosity.

The organization of this paper is as follows. In the next two sections we describe the optical, and near and far-infrared properties of NGC 660 and UGC 1195. We describe the 21 cm radio-synthesis H I line observations (including those of UGC 1195) in Sec. 4, and the CO line observations in Sec. 5. In Sec. 6 we discuss the dynamical situation of the NGC 660 system and present a mass model, and we present our conclusions in Sec. 7.

2. OPTICAL PROPERTIES

The optical morphology of NGC 660 (Fig. 1) is classified as SBa(s)pec by de Vaucouleurs *et al.* (1991, RC3), but our data show that the galaxy has the global characteristics of a gas-rich disk of type ~Sc. Optical images of the galaxy (see Fig. 1, Benvenuti *et al.* 1976; and Young *et al.* 1988; cf. Hodge 1966, 1982) show two distinct morphological components: (1) a bright disk with a major axis position angle of about 45°. It has a barlike inner structure and it is crossed by two prominent dust lanes, one parallel to the major axis, just north of the center, and another, associated with the polar ring, crossing the disk at right angles some 35″ NE of the nucleus. Surface photometry and kinematics show that it is a highly inclined ($i\sim70°$), rotating exponential disk of about 4′ diameter with a bulge, and (2) an outer polar ring with a global axial ratio of 0.39 and a mean P.A. of 170°, inclined about 55° with respect to the disk major axis.

The galaxy was observed on 1992 September 27 in the *B*, *V*, *R*, and *I* bands with the 105 cm Kiso Schmidt telescope, using a 1000×1018 pixel CCD with a 12.′5×12.′7 field of view and a pixel size of 0.″75 square (Yoshida *et al.* 1994). Exposure time was 5 and 30 min/band. The data reduction was performed with the interactive IRAF and SPIRAL (Hamabe & Ichikawa 1992; Ichikawa & Hamabe 1992) image reduction systems, using dome flatfields and standard stars from Landolt (1992). No color corrections were applied, as they are not know yet accurately for the new Kiso CCD camera system, but they are estimated to be small ($\lesssim$0.01 mag in *V*).

The resulting deep *V*-band image is shown in Fig. 1(a) the FWHM seeing is 5.″5. In order to reveal the small-scale structures in the system, we made an unsharp masked image [Fig. 1(b)], by averaging the deep *V*, *R*, and *I* images, in order to improve the signal-to-noise ratio in the faint polar ring, and then subtracting a spatially smoothed version of the map. The masked image shows the prominent dust lanes against the disk (both in the disk plane and the one caused by the polar ring) and small-scale structure throughout the ring. Especially in the *N*-half of the ring, the small structures coincide with the H II regions seen in Fig. 1(d). We obtained color maps, using only pixels above the 3σ level in each map. The $V-I$ color map [Fig. 1(c)] shows two almost equally red ($V-I\sim1.8$ mag) regions in the disk, corresponding to the nucleus and to the most pronounced dust lane associated with the polar ring, crossing the disk some 35″ NE of the nucleus. The color of the polar ring is rather constant ($V-I\sim1.0$), and much bluer than that of the disk, indicating it contains a younger stellar population. In addition, the Hα image [Fig. 1(d)—courtesy of J. S. Young) shows lots of H II regions throughout the disk and the ring, indicating ongoing massive star formation in the accreted matter that formed the ring.

We can use the color of the polar ring to estimate its age. The stars in the ring must have formed out of the gas accreted in the event that caused it, since only the dissipative gas component of the disrupted companion could have settled in a ring, while its stellar component was dispersed as debris. Thus, using a stellar population synthesis model, we can calculate the color evolution of a single-generation stellar population and estimate the age of the ring. We used the population synthesis model of Kodama & Arimoto (1994), which is an improved version of similar models (Arimoto & Yoshii 1986; Arimoto & Bica 1989). The estimated stellar population age depends strongly on the metallicity, but we assume that it is not very different from solar, as the large H I gas mass of the polar ring (4×10^9 $\mathcal{M}_\odot$) indicates it must have been accreted from a fairly large galaxy, and since CO line emission has been detected in the polar ring (Paper I). The mean color of the ring, $V-I\sim1.0$, indicates an age of a few (~2–5) billion years, for a 0.5–1 times solar metallicity.

As the disk is crossed by strong dust lanes, we determined the photometric parameters of the galaxy in the *I* band only, in order to minimize the influence of the dust absorption. We fitted the mean surface brightness, axial ratio, and major axis P.A. of the entire system as function of radius (*R*); see Figs. 1(e)–1(g), where we also indicated at which radii the light distribution is estimated to be dominated by the disk ($R\lesssim70''$) or by the polar ring ($R\gtrsim130''$).

The global luminosity profile of the disk can be well represented by an exponential disk with a scale length of 21″

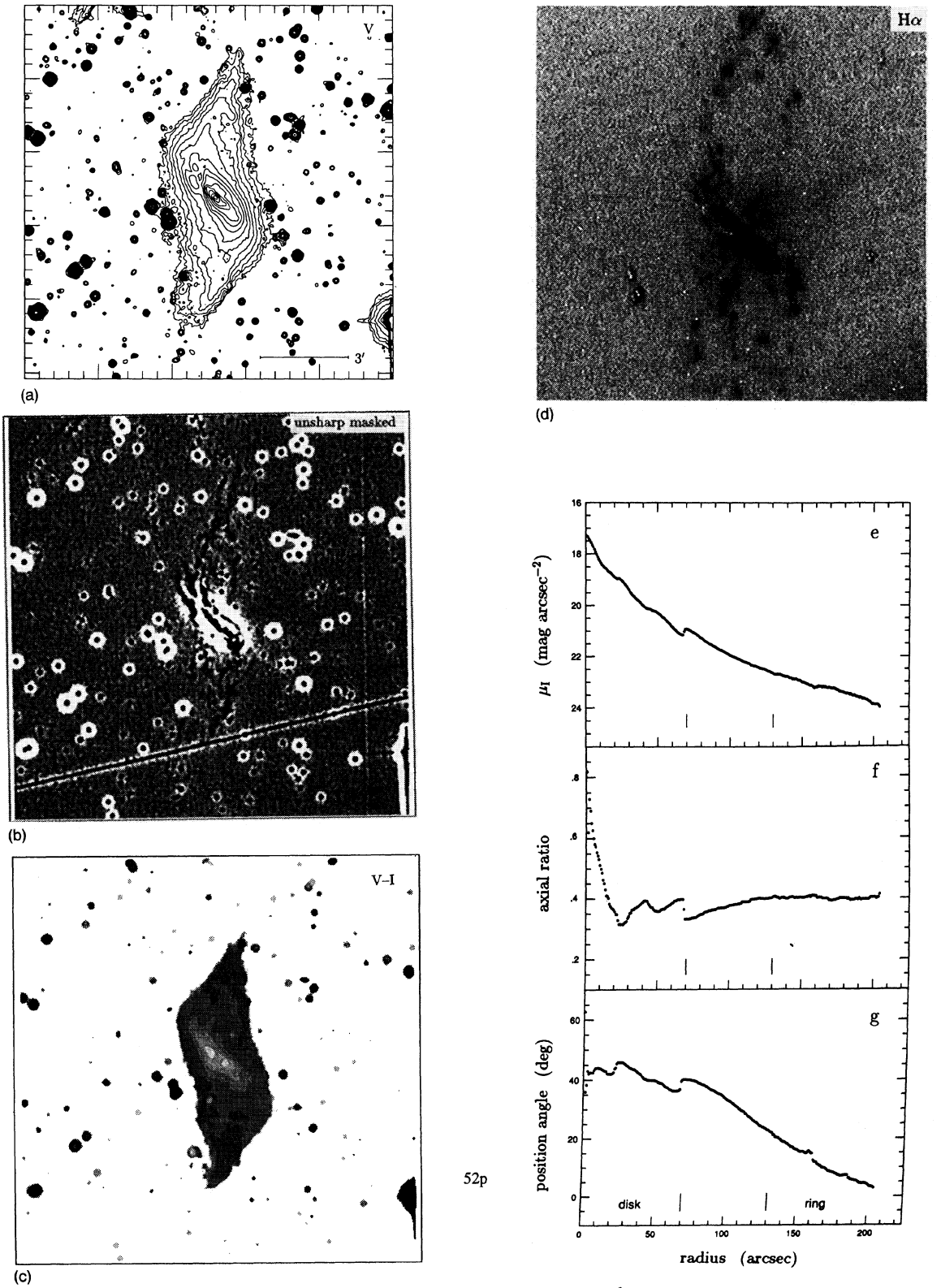

52p

FIG. 1. CCD imaging of NGC 660. (a) *V*-band image. Contours are from 26.0 to 19.5 mag arcsec^{-2}, in steps of 0.5.; image size is 12.5×12.7, (b) unsharp masked average of the *V*, *R*, and *I* images, showing the prominent dust lanes in the disk and the small scale structure in the polar ring; the stripe crossing the frame is caused by a moving object in the *R* band image, (c) *V*−*I* color image. Greyscale steps (from dark to light) are 1.0, 1.2, 1.4, 1.6, and 1.8 mag, (d) Hα image, corrected for continuum emission, image size is 5.8×5.8—courtesy J. S. Young [cf. Fig. 2(b) in Young *et al.* (1988)], (e) mean radial luminosity profile in the *I* band, (f) major axis P.A. as function of radius in the *I* band, and (g) axial ratio as function of radius in the *I* band.

(=1.3 kpc) and a bulge; we could not accurately determine the bulge parameters due to the rather poor seeing, though. The major axis P.A. is rather constant at 42° (comparable to the 45° estimated from near-infrared images, which are basically unaffected by dust). The axial ratio decreases from 0.80 in the center to 0.35 at $R=15''$, and it remains rather constant (0.33) at larger radii, implying an inclination of 71° for a flat disk. The polar ring luminosity profile indicates an exponential scale length of ~62″ (=3.9 kpc), i.e., about three times that of the disk. The axial ratio of the ring is about 0.40 and rather constant with radius. The major axis P.A. increases almost linearly as function of radius, from 158° at $R=130''$ to 177° at 205″. Due to the strong dust lanes in the disk we determined the total luminosity of the polar ring by measuring its total brightness outside the disk and estimating the amount of light from the ring in the region superimposed on the bright disk. This yields a total blue luminosity of $\sim 2.5\times10^9\ \mathscr{L}_{\odot,B}$, about one-third of the total blue luminosity of the NGC 660 system.

The optical spectrum has been studied by Armus *et al.* (1989), Heckman *et al.* (1983), Keel (1983a, 1983b, 1984), and Kennicutt & Pogge (1990), see also Véron-Cetty & Véron (1993). Using the diagnostic diagrams of Veilleux & Osterbrock (1987) we find that NGC 660 has line ratios typical of a LINER-type spectrum in most diagrams (except in [O III]5007/Hβ vs [O I]6300/Hα, where it lies among the "nuclear H II regions"), though there is only an upper limit to the [O III]/Hβ ratio. The FWHM of the Hα line is 186 km s^{-1} (Armus *et al.* 1989). The exact cause of the LINER emission line phenomenon is still controversial: it may be a nuclear starburst or wind, or related to AGNs (e.g., Filippenko 1989; or Heckman 1987).

We obtained optical long-slit CCD spectroscopy of NGC 660 on 1991 October 16 with the 1.52 m ESO telescope, using a Boller & Chivens spectrograph with a 1200 g mm^{-1} grating. The slit width was 1.″8, giving a resolution of 2.2 Å. We made a 1 h exposure along a P.A. of 55°, 10° different from the near-infrared morphological major axis. The data were reduced using the MIDAS system. The spectra were rebinned to a bin size of 0.8 Å over a wavelength range of 4850–6850 Å, and the night sky lines were then subtracted. Gaussian fits were made to the Hα emission line to determine the run of radial velocities along the slit [see Fig. 2(a)], after normalization of the galaxy spectrum along the dispersion direction.

We compared [Fig. 2(a)] our Hα radial velocities to those measured by Benvenuti *et al.* (1976) along a P.A. of about 32° (i.e., 13° to the other side of the major axis). The two datasets are quite different: our spectrum has a ~65 km s^{-1} higher systemic velocity (870 km s^{-1}), a steeper inner gradient, which already starts to flattens out at $R\sim4''$, and a considerably smaller velocity amplitude. From our Hα data we would derive a rotation velocity of only about 110 km s^{-1} [see Fig. 2(b)], if we assume the gas to be in circular rotation in a flat disk inclined 70°, while the data of Benvenuti *et al.* would indicate a rotation velocity of 165 km s^{-1}, and a less steep inner gradient (see Fig. 9). This comparison implies that probably strong noncircular motions occur in the ionized gas. It is therefore not really clear what the true circular

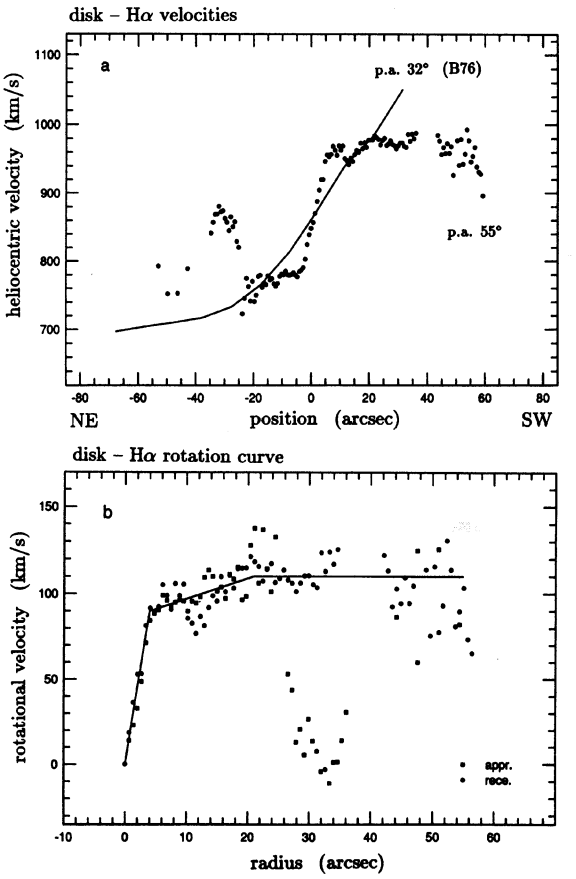

FIG. 2. Hα line velocities in the disk of NGC 660. (a) Hα radial velocities at a P.A. of 55°, 10° from the morphological major axis (45°), together with the average run of Hα velocities measured by Benvenuti *et al.* (1976) at P.A.=32°, corrected to a systemic velocity of 870 km s^{-1}; note the anomalous velocities in the dust lane ~33″ NE of the nucleus, and (b) Hα rotation curve derived from our CCD spectrum (see the text), together with a schematic representation of the curve used in the comparison of rotation curves (Fig. 9).

rotation velocity of the H II gas in the disk is, if it can be derived at all. The rotation curve derived using the data of Benvenuti *et al.* better resembles the H I and CO line data, though (see Fig. 9), which we used for our mass model (Sec. *6.3*).

Radial velocities of about 100 km s^{-1} higher than those seen elsewhere occur ~33″ NE of the nucleus in our CCD spectrum, in the most prominent dust lane associated with the crossing of the polar ring across the disk. These high velocities reflect the, unrelated, rotation of the H II in the polar ring seen against the disk (see Sec. *5.2*), rather than the disk rotation itself—the disk major axis is actually quite close to the minor axis of the ring.

NGC 660 has an irregular-type companion, UGC 1195, which is about four times fainter in the blue. Their projected separation is 21.′8 (=82.4 kpc at the assumed distance) and the H I systemic velocity difference is 74 km s^{-1}, making it plausible that they form a physical pair. They are listed as a pair only by Morgan & Hartwick (1988). NGC 660, with or without UGC 1195, has been listed as a member of a small

group of galaxies by Garcia (1993), Geller & Huchra (1983), Tully (1987), and Vennik (1984, 1986). The group of Geller & Huchra (1983) has a velocity dispersion of 87 km s^{-1}.

3. INFRARED PROPERTIES

We obtained a number of near-infrared images of NGC 660. One was obtained in the J band (1.2 μm) with the 105 cm Kiso Schmidt and a 512×512 PtSi array with a field of view of 14′×11′ and a pixel size of 1.″6×1.″3 (Yanagisawa *et al.* 1994; Ichikawa *et al.* 1994) on 1992 December 31. The total exposure time was 15 min, and the limiting surface brightness is ~22.5 mag arcsec^{-2}. The others (see Fig. 3 [Plates 21–24]) were obtained in the J, H, and K' bands (1.2–2.2 μm) with the ISAS 1.3 m telescope in Tokyo, using the PICNIC 256×256 NICMOS array with a pixel size of about 1.″1 (Kobayashi *et al.* 1994), on 1993 December 25. The total exposure time was 15–28 min/band, the limiting surface brightness is about 23.3–21.6 mag arcsec^{-2} for the $J-K'$ band, respectively, and the mean FWHM seeing is 2.″2.

The PICNIC images show a considerable amount of structure in the disk, see Figs. 3(a) and 3(b); the polar ring is detected only faintly in all near-infrared images. The optically prominent dust lanes are seen best in the J images, and not at all in the K' band. The direct and an unsharp-masked K' band image [Fig. 3(c)], made like Fig. 1(b) (see above), show that the inner bulge is box shaped, as noted previously by Shaw (1993), and that it is surrounded by an X-shaped structure, extending out to about 20″ from the nucleus. These may indicate peculiar stellar orbits in the bulge. The K' image best shows two linear features along the major axis at R~18–40″. It is not clear what these features are, also seen the high inclination of the disk, but they might be related to a barlike structure. We also made a $J-K'$ color image [Fig. 3(d)], using a cutoff of 20.5 and 20 mag arcsec^{-2} in the J and K' image, respectively. The above-mentioned linear features lie on a narrow, almost straight, red band along the disk major axis; they have practically the same color ($J-K'$~1.6 mag) as the narrow red features associated with the optical disk lanes, both associated with the polar ring and parallel to the major axis, but they do not seem to be associated with a dust feature themselves. The nuclear region is quite red ($J-K'$~2.2 mag).

NGC 660 has been detected by the *IRAS* Survey instrument at 2.8, 6.5, 74.7, and 106.4 Jy at 12, 25, 60, and 100 μm wavelength, respectively (Rice *et al.* 1988), while UGC 1195 was not detected (Fullmer *et al.* 1988), from which we estimate conservative upper limits of 1 and 2.5 Jy at, respectively, 60 and 100 μm for this object. From the *IRAS* Survey data we derived far-infrared luminosities $L_{\rm FIR}$ in the 40–120 μm region (see Table 1), using the far-infrared flux parameter FIR (e.g., Helou *et al.* 1989), and assuming a λ^{-1} dust emissivity law. We thus find $\log(L_{\rm FIR}/L_\odot)=10.30$ and $\lesssim 8.5$, and $\log(L_{\rm FIR}/L_B^0)=0.67$ and $\lesssim -0.5$ for NGC 660 and UGC 1195, respectively, as well as a rather high average dust temperature of $T_d=42$ K for NGC 660, similar to the temperature derived for the archetypical starburst galaxy M 82. The beam size of the *IRAS* Survey and CPC instruments is not really good enough to resolve the far-infrared emission of NGC 660 (Soifer *et al.* 1989; van Driel *et al.* 1993). At 11 μm wavelength about 75% of the radiation originates from a region with a diameter of 13″ (=800 pc), elongated along the disk major axis (Werner *et al.* 1986).

TABLE 1. Global optical and far-infrared characteristics.

Object	NGC 660	UGC 1195	Ref.
Position (R.A.)	$01^h40^m20^s.8$	$01^h39^m48^s.0$	RC3,*
Position (Dec.)	13°23′20″	13°43′52″	RC3,*
Morph. classif.	SBa(s)p	Irr?	RC3
	RSbc:p	–	*
Diam. ($D_{25}\times d_{25}$)	8.′3×3.′2	3.′5×1.′1	RC3,UGC
Major axis p.a.	170	50°	RC3
Magnitude B_T^0	11.44	12.91	RC3
Color $(B-V)_T^0$	0.74	–	RC3
$\log(L_B^0/L_{\odot,B})$	9.84	9.26	*
$\log(L_{FIR}/L_B^0)$	0.67	≲-0.5	R,*
$\log(S_{100}/S_{60})$	0.15	–	R
Heliocentric veloc.	823	772 km s^{-1}	RC3,*
Assumed distance	13.0	13.0 Mpc	*

References to TABLE 1.

R: Rice *et al.* (1988)
RC3: de Vaucouleurs *et al.* (1991)
UGC: Nilson (1973)
*: this paper

Adopting a far-infrared dust opacity $\kappa=2.3\times10^4$ cm^2 g^{-1} at 100 μm (Gillett *et al.* 1988), and a single-temperature dust distribution, we would estimate (see, e.g., van Driel & van den Broek 1991) a radiating dust mass $\mathcal{M}_d$ of 2.7×10^5 $\mathcal{M}_\odot$ for NGC 660. However, ground-based observations at 160 to 1300 μm (Chini *et al.* 1986; Rickard & Harvey 1984) show the presence of two dust components in NGC 660, with temperatures of 18 and 51 K, respectively. In this LINER galaxy the luminosity of the warm component, associated with the star-forming regions, is about 1.4 times that of the cold dust, associated with the general interstellar radiation field (Chini *et al.* 1986; cf. Rowan-Robinson & Crawford 1989). An application of a simple two-component (18/60 K) dust model (see de Jong & Brink 1987; van Driel & van den Broek 1991) to the *IRAS* data shows that we underestimate the radiating dust mass by about a factor of 40 if we assume a single dust temperature. Hence, we would estimate a total radiating dust mass of $\sim10^7$ $\mathcal{M}_\odot$ for NGC 660 (compared to 6.5×10^7 $\mathcal{M}_\odot$ estimated by Chini *et al.* 1986), implying a total (H I+H_2) gas-to-dust mass ratio of 700, about a factor 4 higher than the canonical Galactic ratio of 150 (see, e.g., Spitzer 1978); this is a usual value for a galaxy with warm dust (Young *et al.* 1986). The estimated mass depends critically on the assumed temperature of the cold component as well as the dust opacity, though.

Midinfrared spectra, at 8–23 μm, obtained with the LRS spectrograph of *IRAS* (Roche *et al.* 1991; Cohen 1992), show a number of strong absorption lines, which are also seen in other galaxies with optical LINER spectra, and are considered by them to be the result of a starburst.

4. WESTERBORK 21 cm H I LINE OBSERVATIONS

We obtained 21 cm H I line observations with the Westerbork Synthesis Radio Telescope (WSRT), see Table 2. For

TABLE 2. Parameters of radio line observations.

Line Telescope	21 cm H I WSRT	CO(1–0) Nobeyama	CO(2–1) IRAM
Observation date	22 Aug. 1990	Jan. 1987	June 1988
Integration time	12	4	13 hrs
Baselines[1]	48(72)2712 m	–	–
Field center (R.A.)	$01^h40^m21^s$	$01^h40^m21^s$	$01^h40^m21^s$
Field center (Dec.)	13°25′00″	13°22′40″	13°22′40″
Beam HPBW ($\Delta\alpha \times \Delta\delta$)	13″.2×60″.2	17″×17″	12″×12″
Map size ($\Delta\alpha \times \Delta\delta$)	21′×85′	2′.2×2′.2	2′.2×2′.2
Primary beam HPBW	36′	–	–
Central velocity	853	862	862 km s^{-1}
Effective bandwidth	746	1330	665 km s^{-1}
Channel separation	16.5	0.65	1.3 km s^{-1}
Effect. velocity resol.	20	10	10 km s^{-1}
rms noise	1.8	0.030	0.035 K
	1.9 mJy/beam	–	–

Notes to TABLE 2.

[1]: shortest spacing(increment)longest spacing

references to the telescope and the data handling methods see, e.g., van Driel *et al.* (1989). Data were obtained simultaneously in 64 frequency channels over a total bandwidth of about 750 km s^{-1} using a digital spectrometer. The velocity resolution is 20 km s^{-1}, i.e., 1.2 times the channel separation. Bad data points were removed and the remaining data were Fourier transformed into maps of the brightness distribution in each velocity channel. The subsequent data reduction was carried out with the interactive GIPSY system (Allen *et al.* 1985; van der Hulst *et al.* 1992). NGC 660 and UGC 1195 have also been mapped with the VLA (see Gottesman & Mahon 1989) with a similar sensitivity and velocity resolution but a better north–south resolution (beam size 14″.9 ×13″.5, $\Delta\alpha\times\Delta\delta$). Their preliminary results are comparable to ours.

Fifteen channels at the extremes of the bandwidth (V =389–522 and 1152–1235 km s^{-1}) are free of H I line emission and absorption, and they were averaged into a map (Sec. *3.1*) of the 21 cm radio continuum emission, which was then subtracted from all other channel maps (V=538–1135 km s^{-1}).

4.1 Radio Continuum Emission

We CLEANed (Högbom 1974) the above-mentioned average map of the 21 cm radio continuum emission, and found a total flux density of 379 mJy for NGC 660, and a ~9 mJy 3σ upper limit for a point source in UGC 1195, in good agreement with Garwood *et al.* (1987) and Hummel (1980). The NGC 660 source has a 300 mJy central component, resolved in the east–west direction only (intrinsic size 15″), and 80 mJy in an extended structure with a P.A. of about 50° and a size of ~2′. NGC 660 was also mapped with the VLA at 6 and 20 cm with beam sizes between 1″ and 60″ (Condon 1980, 1983, 1987; Condon & Broderick 1988; Condon *et al.* 1982, 1990; Hummel *et al.* 1984, 1987). The observations with the highest resolution (0″.6, Condon *et al.* 1982) show two slightly resolved regions of comparable flux density with a separation of 4″ and a P.A. of 50°. NGC 660 was not detected at VLBI resolution (Jones *et al.* 1981). The total 21 cm radio power of NGC 660 is $\log(P_{1.4}/\mathrm{W\,Hz^{-1}})=21.88$, and the central source in NGC 660 is very strong [$\log(P_{1.4}/\mathrm{W\,Hz^{-1}})=21.78$] for a normal barred galaxy, while the radio power of the disk (21.67) is rather normal (see Hummel 1981). The radio power of UGC 1195, <20.2, is rather low. NGC 660 has a mean radio spectral index α of about −0.57 (Dressel & Condon 1978; Israel & van der Hulst 1983; Garwood *et al.* 1987), indicating the presence of a fair amount of thermal free–free radiation from star-forming regions, if we assume a spectral index of −0.8 for the nonthermal radiation.

4.2 H I Channel Maps and Global H I Content

The full-resolution CLEANed line channel maps of NGC 660, after subtraction of the continuum, (Fig. 4) are shown for V=671–1052 km s^{-1}, where H I emission was visible. They show the two main kinematic components: the disk with a major axis P.A. of ~225°, and the polar ring with a P.A. of ~170°.

We obtained a global H I profile of NGC 660 (see Fig. 5 and Table 3) by integrating the flux density in each channel map over an area covering the entire H I emission, and correcting for the primary beam attenuation. NGC 660 is rich in H I gas ($\mathcal{M}_{\mathrm{H\,I}}/L_B^0 = 0.78\mathcal{M}_\odot/L_{\odot,B}$), almost an order of magnitude more gas rich than other, morphologically normal, galaxies of its morphological type according to the RC3, Sa (e.g., Huchtmeier 1982). However, we estimate that about 75% of the total H I mass (i.e., ~4×10^9 $\mathcal{M}_\odot$) resides in the polar ring, while only about 25% (~1.4×10^9 $\mathcal{M}_\odot$) is found in the disk. This implies a global H I content of about $\mathcal{M}_{\mathrm{H\,I}}/L_B^0 \sim 0.3\mathcal{M}_\odot/L_{\odot,B}$ for the disk, typical for an Sc-type spiral, and of ~$1.7\mathcal{M}_\odot/L_{\odot,B}$ for the polar ring, which would be a very high ratio even for a gas-rich Magellanic-type dwarf galaxy (Huchtmeier & Richter 1988). This, like its molecular gas content (Sec. *5.2*) indicates that the disk is of a later morphological type than Sa.

Ten single-dish H I line profiles of NGC 660 have been published, see Richter *et al.* (1994), and the compilations by Huchtmeier & Richter (1989) and Paturel *et al.* (1990). Our WSRT global profile agrees quite well with them (see Table 3), indicating that there is not too much very extended H I emission around the galaxy, cf. Briggs *et al.* (1980).

4.3 H I Distribution and Kinematics

We made a map (Fig. 6) of the H I column density distribution in NGC 660 from the 28 emission line channel maps (V=605–1052 km s^{-1}) at the full resolution of 13″.5×60″.5, using the so-called conditional transfer method (e.g., Bosma 1981), adding only those pixels where the signal exceeded the 2σ level in the corresponding channel maps smoothed to a 60″×90″ resolution. The map clearly shows the spatially unresolved central H I absorption, and emission from the disk (P.A. 45°) and the polar ring (P.A. 170°).

We made an H I velocity field for NGC 660 (Fig 7.) with a resolution of 13″×60″ by calculating an intensity-weighted mean velocity for each pixel, summing the same masked channel maps used in making the H I column density distribution map. This map shows the regular rotation of the polar

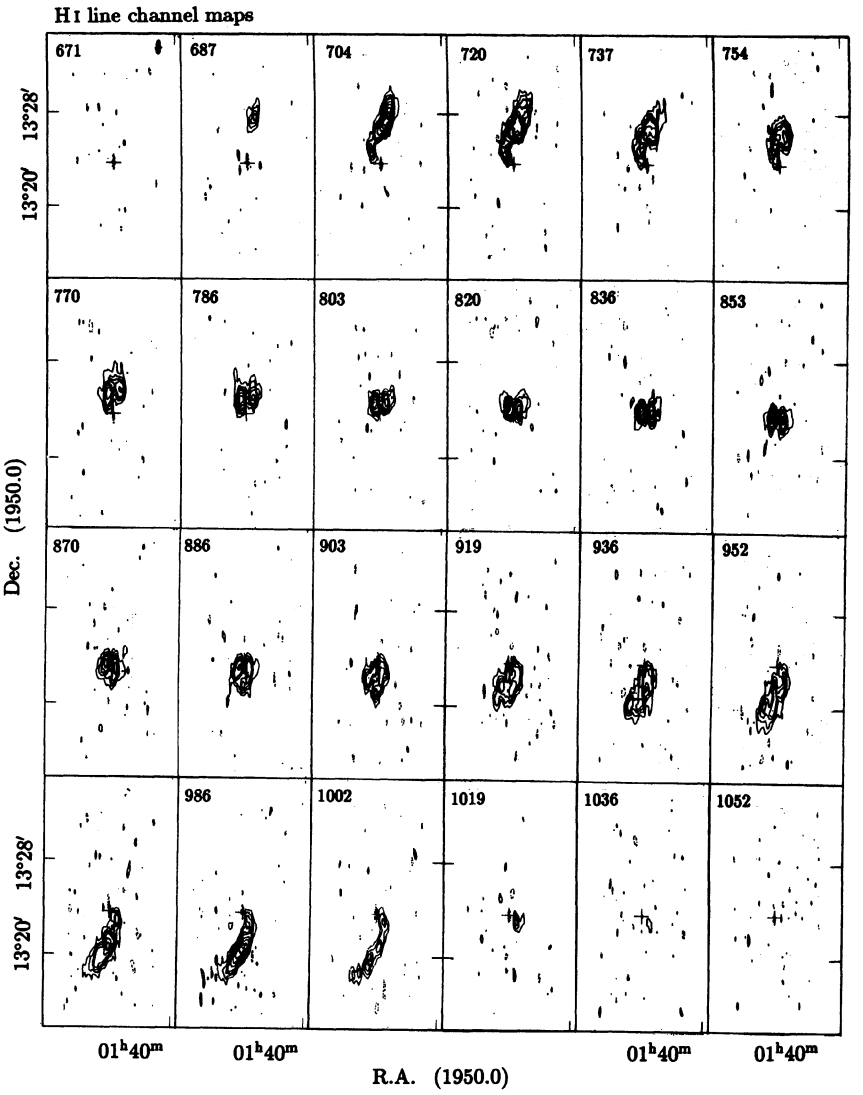

FIG. 4. H I line channel maps of NGC 660 with a resolution of 13″×60″. Contours are −10, −5, 5, 10, 15, 20, 30, 40, 50, and 60 mJy/beam, negative contours are dashed; the rms. noise is 2 mJy/beam. The central velocity of each map has been indicated, and the HPBW is shown by the hatched ellipse in the upper left map. The cross indicates the optical center of the galaxy (Table 1).

ring; the distortion of the isovelocity contours near the minor axis is due to the superposition of the two distinct kinematic systems (disk and polar ring), see below.

H I position-velocity plots are shown along two position angles: Fig. 8(a) made along the mean kinematical major axis of the polar ring (P.A. 170°), clearly shows the rotation of the ring, as well as the nuclear H I absorption (see below). Figure 8(b) (cf. Fig. 7 in Gottesman & Mahon 1989), made along the major axis of the disk (P.A. 45°), shows the disk, represented by the maxima at the extreme velocities, as well as the polar ring, i.e., the two maxima closer to the center near the systemic velocity. The inner disk H I rotation curve (Fig. 9) is confused by the strong emission from the polar ring and the nuclear absorption, but it is rather flat at $v_{\rm rot}\sim150$ km s^{-1} from $R\sim30''$–$90''$, if we assume circular rotation in a disk with an inclination of 70°, in agreement with the rotation velocities derived from the CO line data (see Sec. *4.1* and Fig. 9), and in between the rotation velocities of about 110 and 240 km s^{-1} derived from Hα spectra (see Secs. 2 and *7.2*). From the CO and H I rotation curves we estimate a total mass of about $3.5\times10^{10}\mathcal{M}_\odot$ for the disk within $R=6.3$ kpc (about R_{25}), assuming a simple spherical mass model ($\mathcal{M}_T=V_{\rm rot}^2\,R/G$), implying an estimated total disk mass-to-light ratio of $\mathcal{M}_T/L_B^0\sim7.5\mathcal{M}_\odot/L_{\odot,B}$ within this radius, a normal value for a spiral galaxy at such a radius (e.g., van Driel & van Woerden 1991).

The position-velocity plots also clearly show the H I absorption against the central source, at a somewhat broader velocity range ($V\sim650$–1070 km s^{-1}) than the H I emission. The inverted double horn shape of the H I line absorption profile, seen also in the OH and H_2CO profiles (Baan *et al.* 1986, 1989, 1993; Claussen & Lo 1986; Henkel *et al.* 1986;

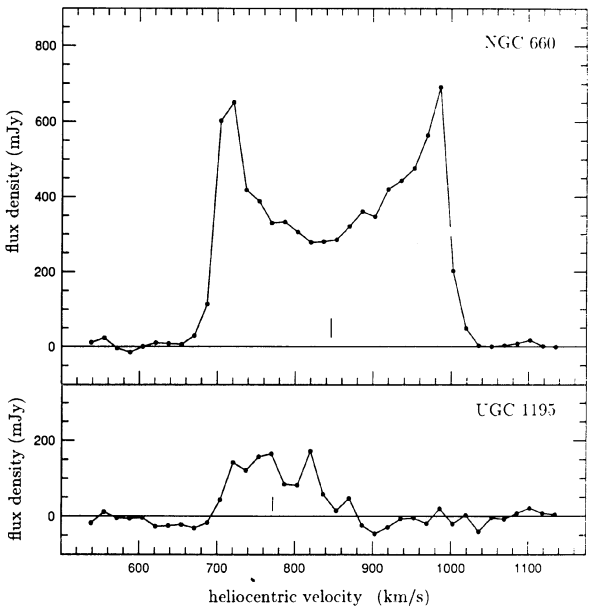

FIG. 5. Global H I line profiles of NGC 660 and UGC 1195, made as explained in the text. The H I systemic velocities (Table 3) have been indicated. The error bars show the typical uncertainty in the data.

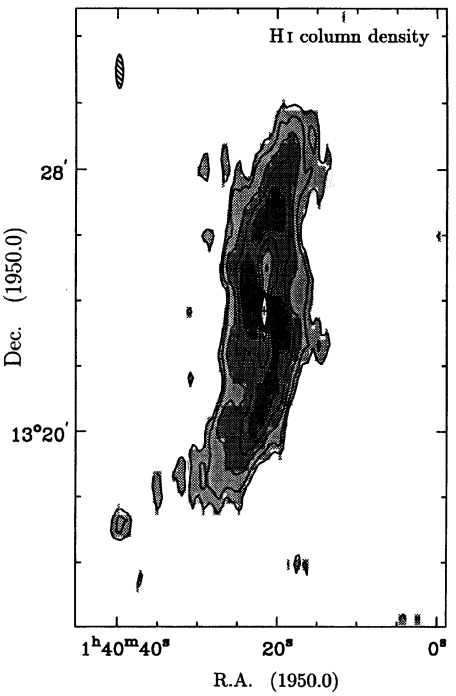

FIG. 6. H I column density distribution of NGC 660 with a resolution of of 13″×60″ ($\Delta\alpha\times\Delta\delta$), made as explained in the text. Contour levels are 0.4, 0.8, 1.7, 2.9, 4.2, 5.5, and 6.7×10^{21} cm^{-2}. The beamsize is shown by the hatched ellipse. The cross indicates the optical center of NGC 660.

Rickard *et al.* 1982) apparently shows the absorption against the two compact nuclear continuum sources (see Condon *et al.* 1982, Sec. *3.1*) and thus reflects the rotation of the gas in the innermost regions ($R\sim2''$). The H I absorption has been slightly spatially resolved by Gottesman & Mahon (1989) with a beam of 12″, indicating a very sharp rising H I rotation curve, consistent with the Hα and CO line data. High-resolution OH and H I absorption line observations against the nucleus of NGC 660 (Baan *et al.* 1992) also reflect the disk and ring kinematics. If we assume that the H I gas seen in absorption rotates in circular orbits in the disk ($i=70°$), we would derive $V_{rot}\sim200$ km s^{-1} at $R\sim2''$, about 4.5 times higher than the Hα velocity observed there (Sec. *2.1*).

Since the standard algorithms for the derivation of rota-

TABLE 3. Global H I properties.

Object	NGC 660	UGC 1195	Ref.
$\int SdV$	135	17.5 Jy km s^{-1}	*
	150.3	22.7 Jy km s^{-1}	R,GS
M_{HI}	5.37	0.70 10^9 $M_\odot$	*
M_{HI}/L^0_B	0.78	0.39 $M_\odot/L_{\odot,B}$	*
Heliocentric velocity	846	772 km s^{-1}	*
	852	774 km s^{-1}	R,GS
Profile width W_{50}	304	122 km s^{-1}	*
Profile width W_{20}	322	143 km s^{-1}	*
	320	157 km s^{-1}	R,GS
Continuum flux density $S_{1.4}$	379	<9 mJy	*
Radio power log($P_{1.4}$/W Hz^{-1})	21.88	<20.2	*

References to TABLE 3.

GS: Giovanardi & Salpeter (1985)
R: Rots (1980)
*: this paper

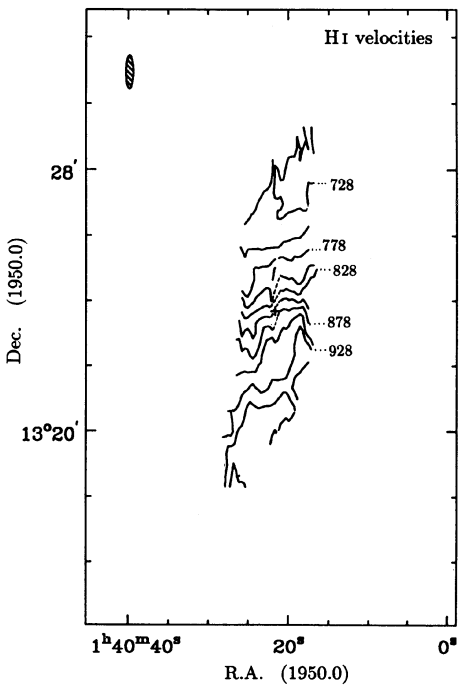

FIG. 7. H I velocity field of NGC 660, made as explained in the text. The dotted lines are linear interpolations between drawn contours in regions of low H I column density. The beam size of 13″×60″ is shown by the hatched ellipse. The cross indicates the optical center of the galaxy.

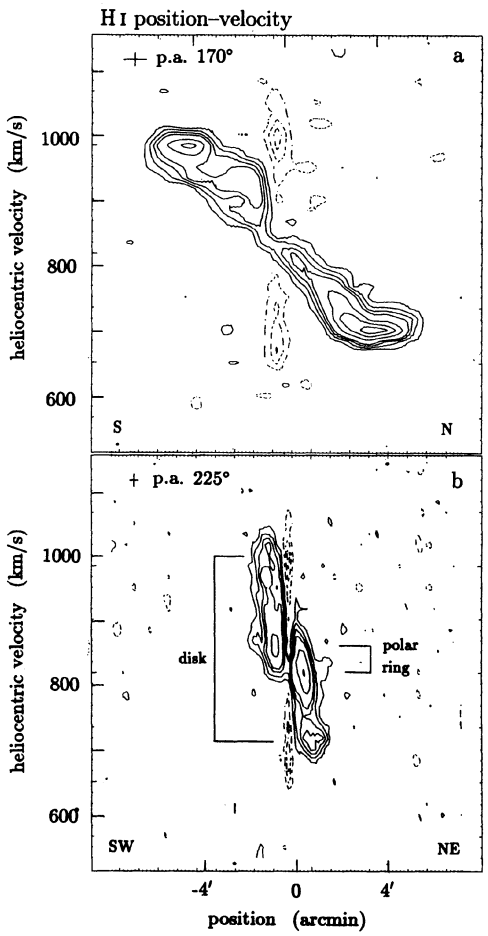

FIG. 8. H I line position-velocity plots of NGC 660. Contours are −12, −8, −4, 4, 8, 12, 16, 24, and 40 mJy/beam, negative contours are dashed; the rms noise is 2 mJy/beam. The FWHM resolution has been indicated by a cross in each plot. (a) At the major axis P.A. of the outer polar ring (170°), resolution 60″×20 km s^{-1}, and (b) at the major axis P.A. of the disk (225°), resolution 19″×20 km s^{-1}.

tion curves from a velocity field (Warner *et al.* 1973; Begeman 1989) cannot be applied to this peculiar galaxy, we instead derived the polar ring rotation curve using a three-dimensional geometrical model (see Paper I) fitted to the optical and H I morphology and kinematics, assuming an inclination of 82° for the ring on the plane of the sky. The resulting velocities are shown in Fig. 9, together with various disk rotation curves. The polar ring rotation curve is slightly rising, from 106 km s^{-1} at R=9 kpc to 127 km s^{-1} at 18 kpc. From it we derive a total mass of $6.8\times10^{10}\mathcal{M}_\odot$ within R=18 kpc, using a simple spherical mass distribution, implying a total mass-to-light ratio of $10.\mathcal{M}_\odot/L_{\odot,B}$ for the entire galaxy within this radius. This mass is close to $5.8\times10^{10}\mathcal{M}_\odot$, the total mass of the system derived from our mass model fitting (Sec. *6.3*). Another estimate of the (minimum) mass of NGC 660 is $5\times10^{10}\mathcal{M}_\odot$, based on the assumption that the NGC 660/UGC 1195 pair is gravitationally bound.

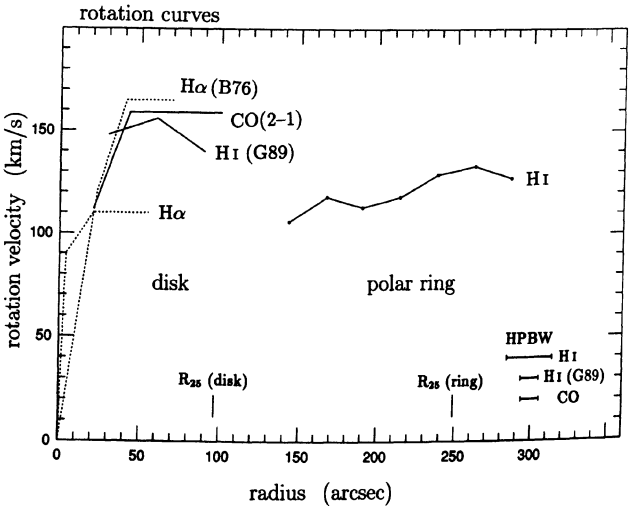

FIG. 9. Rotation curves of the disk and polar ring of NGC 660, made as described in the text. Disk: indicated schematically are the rotation curve based on our major-axis Hα spectrum and the Hα spectrum of Benvenuti *et al.* (1976) (B76), the H I line major axis position-velocity plot (GM89) of Gottesman & Mahon (1989), and our CO(2–1) line velocity field (see Fig. 19). All curves were derived assuming circular rotation in a flat disk inclined 70°. Polar Ring: rotation curve based on our H I line data, using a three-dimensional geometrical model. Also shown are the optical R_{25} radius of the disk and the polar ring, as well as the mean beam sizes of the H I and CO line observations.

4.4 UGC 1195

With the WSRT we also detected the Irr? galaxy UGC 1195 (Fig. 10), some 20′ from the pointing center, where the primary beam efficiency is about 45%. No radio continuum emission was detected from it (see Sec. *3.2*). Our rather noisy H I profile (Fig. 5 and Table 3) agrees fairly well with the published single-dish profiles, see Lu *et al.* (1993), and the catalogs of Huchtmeier & Richter (1989) and Paturel *et al.* (1990). We find an H I mass of $7\times10^8\mathcal{M}_\odot$, and a gas content of $0.4\mathcal{M}_\odot/L_{\odot,B}$, which is rather low for an irregular-type galaxy.

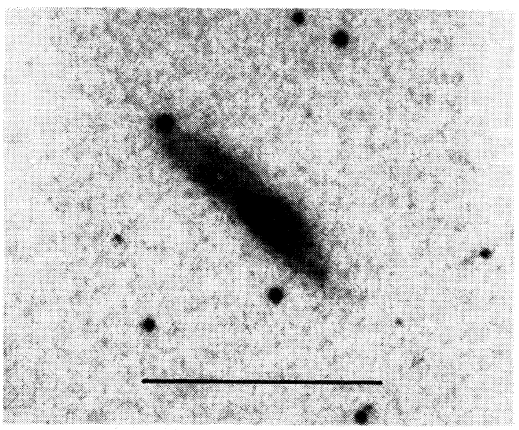

FIG. 10. Photograph of UGC 1195, from a blue Palomar Sky Survey print. The bar indicates a scale of 3′.

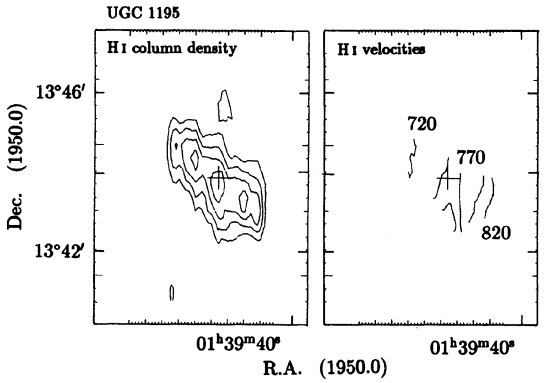

FIG. 11. H I column density distribution and velocity field of UGC 1195 with a resolution of 13″×60″ (indicated by the hatched ellipse), made as explained in the text. (a) H I column density map. Contours are 6.2, 12.4, 18.7, and 24.9×10^{20} cm^{-2}, corrected for the primary beam attenuation. (b) H I velocity field. The cross indicates the optical center of the galaxy (Table 1).

The H I column density distribution, velocity field, and major axis position-velocity plot (Figs. 11 and 12), made in a similar way as for NGC 660, show that this is a galaxy with an H I distribution almost as large as the optical outlines, and with undisturbed kinematics. We estimate a low rotational velocity of 56 km s^{-1} at R=1.7 (=6.4 kpc, or ~R_{25}), assuming an inclination of 72° (UGC), which implies a total mass of 4.7×10^9 $\mathcal{M}_\odot$ and a low $\mathcal{M}_T/L_B^0$ ratio of 2.6$\mathcal{M}_\odot/L_{\odot,B}$ within R=6.4 kpc, about a factor of 3 lower than the average value found for normal spirals at such a radius (van Driel & van Woerden 1991).

5. CO LINE OBSERVATIONS

We mapped the disk of NGC 660 in the ^{12}CO(2–1) line with the 30 m IRAM telescope and in the ^{12}CO(1–0) line with the 45 m Nobeyama (NRO) telescope with a HPBW of 12″ and 17″, respectively, as well as parts of the polar ring in the CO(2–1) and (1–0) lines at IRAM with a HPBW of 12″ and 22″, respectively. For technical details concerning the NRO and IRAM observations we refer to Gerin *et al.* (1988) and Casoli *et al.* (1990), respectively. To calibrate the data from the two telescopes we also observed several points in the disk in the CO(1–0) line at IRAM, and convolved the NRO CO(1–0) data to the same resolution. To get the same main beam temperatures with both telescopes, we had to multiply the NRO data by a factor 1.4. The temperature scale used throughout this paper is the main beam scale. We used several AOS backends for the CO(1–0) observations, with a resolution of 0.65 km s^{-1}, and a filter bank of 1.3 km s^{-1} resolution for the CO(2–1) data; however, since the lines are relatively broad (100–500 km s^{-1}), we smoothed the spectra to a 10 km s^{-1} resolution in order to increase the signal-to-noise ratio. Here we will limit ourselves to a description of the disk observations, for a discussion of the polar ring observations we refer to Paper I.

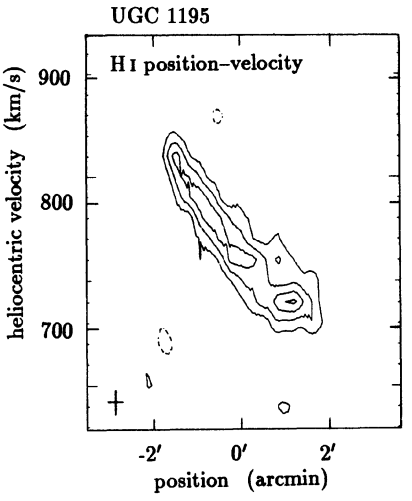

FIG. 12. H I line position-velocity diagram along the major axis of UGC 1195 (P.A. 225°). Contours are −4, 4, 8, 12, and 16 mJy/beam, negative contours are dashed. The rms noise is 2 mJy/beam. The cross indicates the resolution (19″×20 km s^{-1}).

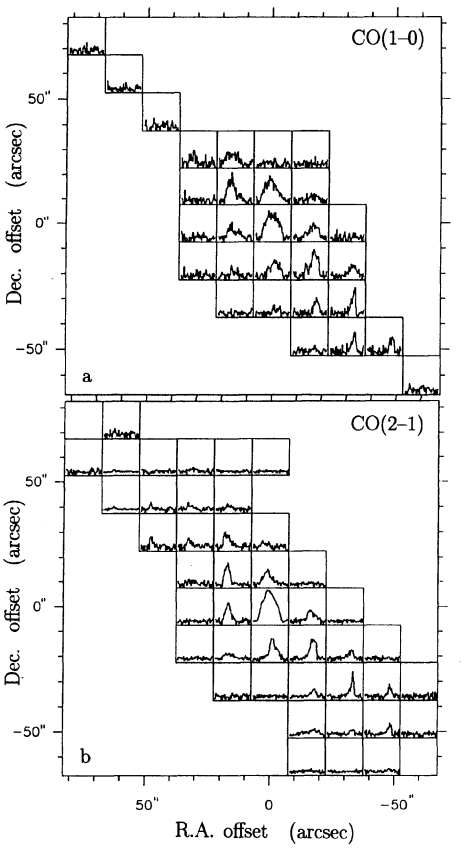

FIG. 13. Mosaic of CO line spectra. Sampling spacing is 15″, velocity resolution is 10 km s^{-1}. The abscissae of the spectra are heliocentric velocities (500–1200 km s^{-1}), the ordinates are T_{mb} (−0.1–0.8 K). Center position (offset 0″,0″) is 01^{h}40^{m}21^s.7,+13°23′40″. (a) CO(1–0) spectra obtained at NRO, HPBW 17″, and (b) CO(2–1) spectra obtained at IRAM, HPBW 12″.

5.1 CO Distribution and Kinematics

The CO spectra are displayed in Fig. 13, and the column

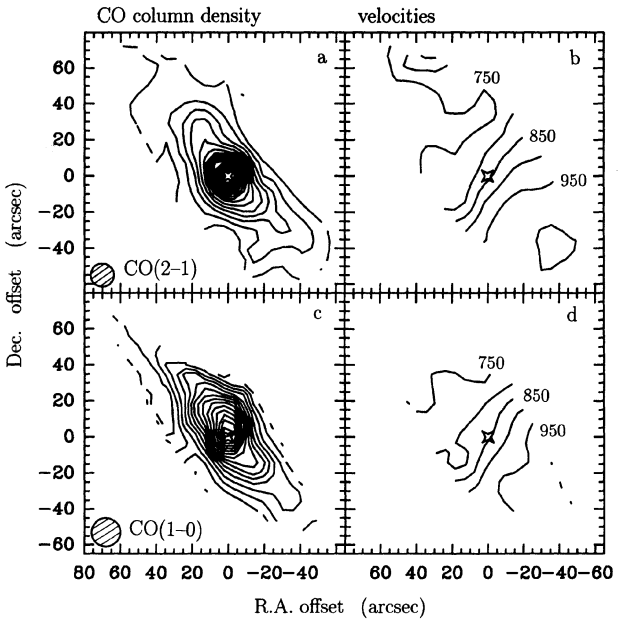

FIG. 14. CO column density distributions and velocity fields. Column density contour levels are from 5 to 200 K km s^{-1} in steps of 12 K km s^{-1}. The hatched circles show the beam sizes. For the center position, see Fig. 13. (a) and (b) CO(2–1) line, IRAM; (c) and (d) CO(1–0) line, NRO.

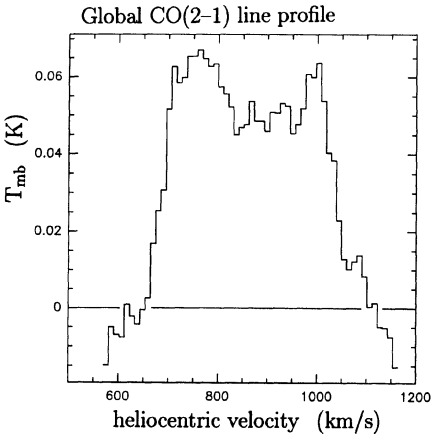

FIG. 15. Total CO(2–1) line emission spectrum of the entire disk area mapped.

density maps in Fig. 14. The molecular gas is clearly associated with the disk, and the concentration in the center is particularly high; half of the molecular mass is contained within $R=20''=1.3$ kpc. As discussed in Paper I, there is also some CO emission associated with the polar ring in the disk area, but it is much weaker than the disk emission. The maximum H_2 surface density in the disk is $\sim 6\times10^{22}$ cm^{-2}, using an N(H_2)/I(CO) conversion ratio of 3×10^{20} cm^{-2}/K km s^{-1} (e.g., Young & Scoville 1991). This is a lower limit to the true maximum, however, since the nuclear disk feature is diluted by the 12″ beam. Our spectra agree, within the errors, with the observation of the NGC 660 center with a 45″ beam by Sanders & Mirabel (1985).

Channel maps obtained in the two CO lines (Fig. 16) clearly show the disk rotation along a P.A. of ~45°. A warping of the CO plane is suggested in the NE region, but this could be due to molecular gas in the polar ring (see Paper I).

To compare the CO(2–1) and CO(1–0) line intensities, and to gain insight in the CO line excitations, we convolved the central CO(2–1) spectra to the NRO beam of 17″; they are very similar to the NRO spectra shown in Fig. 13. The average CO(2–1)/(1–0) ratio in this region is 0.9, with a central maximum of 1.3, a typical value for a spiral galaxy (Braine & Combes 1992; Braine *et al.* 1993). This reflects only the average of the ratio over the entire velocity range, however, and it is clear that there are large variations (from 0.3 to 2) in the ratio as function of velocity, see Fig. 17. This implies that the CO excitation can vary from cloud to cloud, suggesting a variety of physical conditions, temperature, density, and optical depth. On average, however, the emission is dominated by standard, optically thick clouds, like those observed in the Milky Way.

We made CO(2–1) and CO(1–0) velocity fields (Fig. 14) by fitting Gaussians to the individual line profiles, as well as a position-velocity diagram in the CO(2–1) line along the disk major axis (Fig. 18). On the NE side the velocities tend to decline at larger radii, while the velocity gradient remains rather flat on the SW side. The range of CO velocities in the inner regions correspond with the range over which H I line absorption is seen against the compact central double radio source (Sec. *4.1*).

We also derived a CO line rotation curve (Fig. 19) using mean velocities derived for each spectrum by fitting a Gaussian, avoiding a sector of ±45° around the the minor axis, and assuming a major axis P.A. of 45° and an inclination of 70°. The curve rises from 110 km s^{-1} at $R=20''$ towards ~160 km s^{-1} at 45″–100″ radius. The profiles indicate that the maximum rotation velocity occurs near the center, in an unresolved region of <5″ in radius. The CO rotation curve appears to have a high central peak, followed by a gap and then a rise, a behavior typical of central noncircular motions; also the major axis CO line position-velocity plot (Fig. 18) hints at this tendency.

5.2 H_2 Mass and Star-Formation Efficiency

NGC 660 is a galaxy rich in cold interstellar gas. Like the optical and H I line data, also the CO line data indicate that the disk of NGC 660 is of a later morphological type than the SBa classification from the RC3. From the total CO(1–0) profile of the disk (Fig. 15) we derive a total H_2 mass of $3.7\times10^9 \mathcal{M}_\odot$, using the above-mentioned H_2/CO conversion factor, and assuming a CO(2–1)/(1–0) integrated line intensity ratio of 0.9 averaged over the entire area mapped in both lines. The H_2 gas content of the disk is high, $\mathcal{M}(H_2)/L_B^0 \sim 1.6 \mathcal{M}_\odot/L_{\odot,B}$. Using a dynamical disk mass of $3.5\times10^{10}\mathcal{M}_\odot$ (see Sec. *4.3*, following, Rubin *et al.* 1985), we find an $\mathcal{M}(H\ I + H_2)/\mathcal{M}_{dyn}$ ratio of 0.15 for the NGC 660 disk, which is typical for an Sbc type spiral (Young & Scoville 1991). The $H_2/H\ I$ mass ratio of the disk, 2.7, is

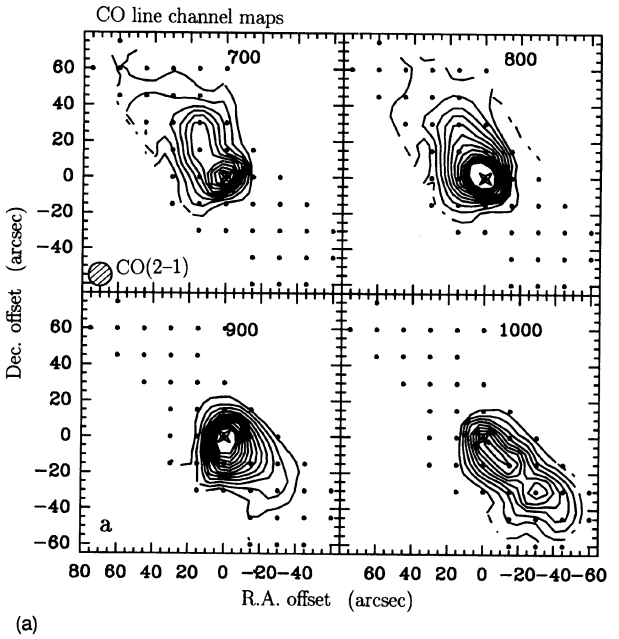

(a)

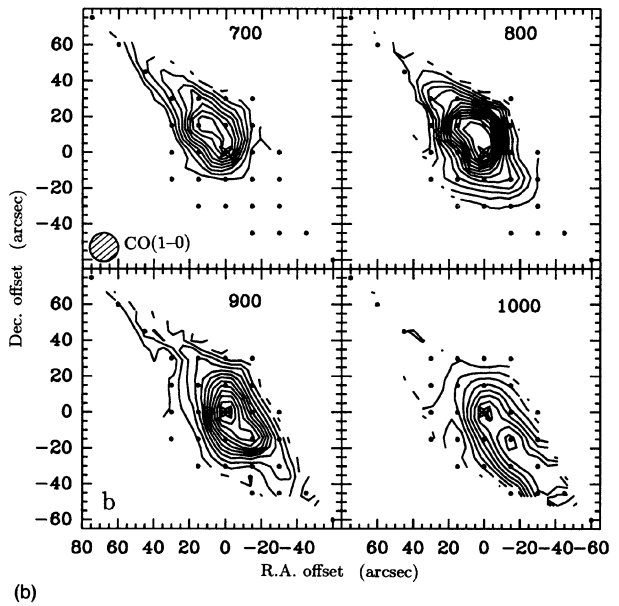

(b)

FIG. 16. CO line channel maps of 100 km s^{-1} width, centered at 700, 800, and 900 km s^{-1}. Contours are from 2 to 50 K km s^{-1} in steps of 4 K km s^{-1}. The dots show the pointing centers of the profiles. For center position, see Fig. 13. (a) CO(2–1) IRAM, and (b) CO(1–0) NRO.

typical for an S0/Sa type galaxy, but such high molecular/atomic mass ratios are even found in some Sc disks (Young & Scoville 1991).

The global $L_{\rm FIR}/\mathcal{M}_{\rm H_2}$ ratio of NGC 660 is 5.4 $L_\odot/\mathcal{M}_\odot$, implying an average "star-formation efficiency," which is virtually independent of Hubble type (e.g., Young & Scoville 1991), typical for a normal (nonstarburst) spiral, i.e., about a factor of 5 lower than the star-formation efficiency of classical starburst galaxies like M 82.

The most striking feature of the molecular gas distribution is the high central concentration; there is an intensity contrast

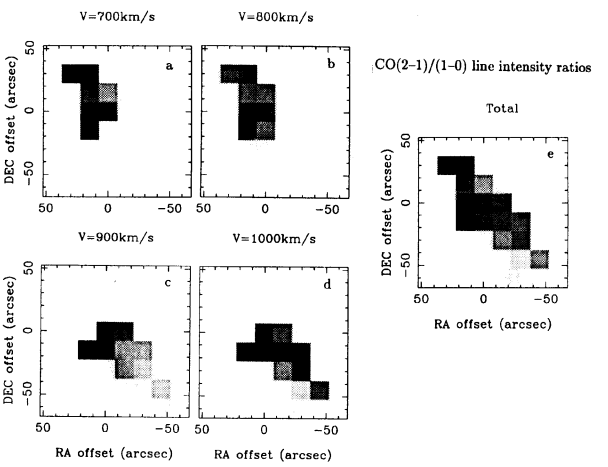

FIG. 17. Greyscale representation of the CO(2–1)/(1–0) line intensity ratio from data convolved to a 17″ resolution. For center position, see Fig. 13. (a)–(d) The line ratio computed within 100 km s^{-1} wide velocity channels centered at 700, 800, 900, and 1000 km s^{-1} (cf. Fig. 16), respectively, and (e) integrated over all velocities.

of almost a factor 10 between the nuclear component and the outside disk. The inner H_2 gas probably resides in a nuclear disk, judging from its dynamics. The presence of such a large quantity of molecular gas in such a small volume can explain the presence of a central starburst region, if this is what actually causes the LINER spectrum. If so, the nuclear molecular clouds must have accumulated in a relatively short time, because of the dispersive effect of a starburst. Given the recent interaction experienced by NGC 660, it is likely that gravitational torques are responsible for driving the gas

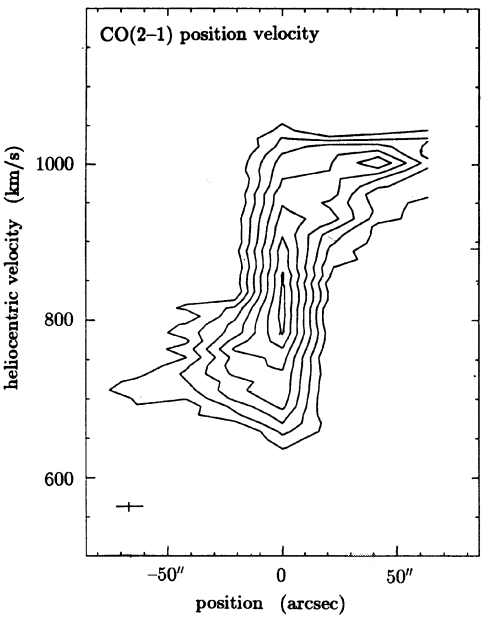

FIG. 18. CO(2–1) line position-velocity plot along the major axis of the disk of NGC 660 (P.A. 45°). Contours are 0.1–0.7 K, in steps of 0.1 K. The cross indicates the resolution of 12″×10 km s^{-1}.

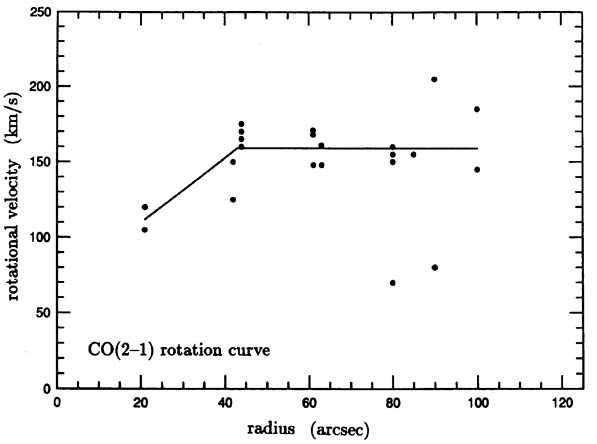

FIG. 19. CO(2–1) rotation curve, made as described in the text. Also indicated is the schematic representation of the data used in the comparison of rotation curves (Fig. 9).

(e.g., Combes 1988; Combes & Gerin 1985). The effect of the possible nuclear starburst and the merging process, on the molecular gas can also be seen in the high $^{12}CO/^{13}CO$ line intensity ratio measured in the CO(1–0) line with a 33″ beam (Aalto *et al.* 1991), which indicates a decrease in the optical depth of the disturbed clouds, or a redistribution of the gas (Casoli *et al.* 1992).

6. DISCUSSION

NGC 660 is a unique, nearby polar ring galaxy, with its inclined, warped, and twisted ring and its gas-rich disk. We will discuss various aspects of the formation and stability of such a system, as well as a bulge/disk/ring/dark halo mass model.

6.1 NGC 660—A Peculiar Polar Ring Galaxy

The presence of a polar ring strongly suggests that NGC 660 has accreted a lot of gas during an interaction with another galaxy. The event probably occurred a few billion years ago, estimating from the stellar population in the ring, which was formed out of the accreted gas, and massive stars are apparently still being formed in the ring, according to the Hα image [Fig. 1(c)].

The geometrical model presented in Paper I indicated that the polar ring of NGC 660 is not quite like the classical examples of such rings, which tend to be rather thin, straight features, usually nearly perpendicular to the disk, since it shows a rather large twist, as well as a substantial warp and a large inclination. Also, the gas-rich disk of NGC 660, with its LINER activity, is quite different from the quiescent, gas-poor S0-type disk found in most polar ring galaxies. The disk of NGC 660 has a total cold hydrogen gas mass of about $5\times10^9\mathcal{M}_\odot$ and a strong central concentration of molecular gas, while the H I distribution of other polar ring galaxies mapped (MCG 5-26-86, II Zw73, and NGC 4650A) shows H I concentrated in the ring only, and a disk devoid of H I gas (Schechter *et al.* 1984; van Gorkom *et al.* 1987). Though there is some evidence (Wakamatsu 1993, and references therein) that the accreted gas triggered some mild nuclear activity in the S0-like disks of some polar ring galaxies, judging from the weak H II and [O III] lines observed, such activity is nothing compared to the vigorous massive star formation seen in NGC 660.

The NGC 660 system was apparently formed in a dramatic collision between two equally massive objects a few billion years ago. The estimated total (stellar+gaseous) present-day mass of the disk is about $2\times10^{10}\mathcal{M}_\odot$, while the polar ring mass is $1.5\times10^{10}\mathcal{M}_\odot$ (see Sec. *6.3*). Note that the latter is an underestimate of the total mass of the erstwhile companion, since in such a collision only the gas can dissipate energy and form an accreted disk, while the stellar component of the companion is scattered into a large volume. The kinematics of the disk, which is optically still heavily scarred by dust lanes, appear to be relatively unperturbed, though it would be hard to spot minor disturbances in such a highly inclined disk. However, the polar ring is now in equilibrium, and almost axisymmetric, in which case the only perturbation in the disk caused by the ring is to make the potential triaxial, like the presence of a weak bar in the disk, which is not expected to severely disturb its internal motions.

The stability of the NGC 660 system is puzzling, as mentioned in Paper I. The disk is undoubtedly an oblate, rotating spiral galaxy, with an apparently stable polar ring in orbit around at an inclination varying from 34° at 9 kpc radius to 56° at 18 kpc. The rotating ring is forced to precess around the pole, due to the flatness of the potential, but the precession rate varies with radius, making the ring disappear quickly by phase wrapping. In Paper I we estimated precession periods varying from 1.1 to 3.6×10^9 yr in the polar ring, and a lifetime for the structure of at most $\sim10^9$ yr. We now estimated an age of a few (~2–5) times 10^9 yr for the ring from its color (see Sec. *2.1*), so a stabilizing mechanism must exist which makes the entire ring precess as a solid body. This could be in principle either a tumbling bar in the disk, or radiative cooling in a polar ring warped towards the equator, but neither of these mechanisms seem appropriate. A third mechanism, self-gravity of a massive polar ring (Sparke 1986) seems to be more successful, since the ring in NGC 660 has a large mass (about 25% of the modeled total mass, and 45% of the total gas mass), and it warps towards the pole. According to Sparke's models, the polar ring needs to have a mass similar to that of the disk in order to stabilize itself, but the models of Dubinski & Christodoulou (1994) indicate that polar rings are already stable against differential precession for a ring mass of only 0.02 times that of the enclosed disk. Our mass model (Sec. *6.2*) indicates that even the former condition for ring stability is satisfied in the case of NGC 660.

An alternative model (Wakamatsu 1993) for the formation of polar *rings*, rather than disks, uses supersonic shock waves generated in the accreted gas, which can remove gas from the inner parts of the ring. Such shock waves can occur within a radius of about 4.5 times the exponential scale length of the inner disk. In the case of NGC 660 this would correspond to about 95″, which is in fact the size of the hole

in the ring measured from the H I map of Gottesman & Mahon (1989), which have a better N–S resolution than ours.

6.2 Polar Ring Mass Models and the Shape of the Dark Halo

One of the great interests in polar ring studies is to attempt a determination of the three-dimensional shape of the galactic potential, in particular the flattening of the dark halo. In principle, polar rings are ideal probes for this, because of their large radii and high inclinations from the plane of the principal (inner) rotating disk. If the flattened potential is asymptotically isothermal and scale free, its derivatives along the r or z axis are the same; but the closed polar orbits followed by the gas will not be circular, with their major axis along the z direction. Using the shooting method we can find the closed orbits at any radius in a given potential, though, and derive the ratio between the polar and equatorial rotation velocities (Katz & Richstone 1984). This ratio $V_{\rm pol}/V_{\rm equ}$ can vary between 0.9 and 0.6 for halo axis ratios between 0.8 and 0.2. It should be noted that the equipotentials are much rounder than the luminosity isophotes, which makes a moderate flattening of the halo hard to see.

Thus, in a flattened potential the orbits in the polar ring would be elongated and the rotation velocities at the pole would be lower than at a similar radius in the equatorial plane. However, the problem is that we cannot compare the rotation velocity of the gas in the polar ring to that of gas in the disk at similar distances from the center, since the ring is (much) bigger than the disk and there is no overlapping range of radii in their rotation curves (see Fig. 9). Thus, we cannot directly determine the flatness of the halo. This must be true in general for any polar-ring system. If there is already gas in the equatorial plane, then accreted gas at the same radii will never settle in a polar ring, as gas cloud collisions with the perpendicular stream will prevent this.

A few polar ring galaxies have been studied in detail: the rotation curve of the main disk is obtained through absorption lines, the polar ring kinematics in the Hα line, and dynamical models are fitted. But the final results are controversial. Nearly round-shaped halos were indicated in studies (Schweizer *et al.* 1983; Whitmore *et al.* 1990), which rely on the hypothesis that the polar rings begin just at the outer optical radius of the main body, or on the extrapolation that the equatorial rotation curve is flat. Also, the uncertainties in the determination of the disk rotation curves are large. The rotation velocities in the equatorial plane (disk) usually can be derived from stellar absorption lines only in these gas-free S0-type disks, which includes an estimated correction for the asymmetric drift. Since the velocity dispersion in the stellar component is quite high, the correction to estimate the true circular velocity is significant. In fact, the most complete modeling of the potential of a polar ring galaxy, NGC 4650A (Sackett & Sparke 1990), which includes a bulge, disk, axisymmetric dark halo and a polar ring, hints the halo is probably flattened, but the data are compatible with a wide range of halo shapes with flattenings between E0 and E8, i.e., from spherical to highly flattened.

The determination of the halo flattening is prevented, however, by an effect intrinsic to polar ring formation. The material in polar orbits is restricted to a narrow annulus, which is either orbiting around the main body, outside the optical disk (as in NGC 4650A or A0136-0801), so the equatorial velocities are not determined at the same radius as the polar ones, or the annulus is within the optical disk (as in ESO 415-G26), but then the dark matter is not predominant, and the visible bulge-to-disk mass ratio will determine the shape of the potential. Of course, the ideal situation would be to measure equatorial and polar rotation curves in H I gas at the same radii, external to the optical disk, but such a situation, involving two perpendicular gas streams, is not stable. In NGC 660 the two gaseous structures, disk and polar ring, are external to each other as well. Another difficulty, due to an observational bias, is that most of detected polar rings are (nearly) edge on, in which case the observed velocity along the major axis is only an indirect indication of the rotation curve, being the average of all projected velocities along the line of sight. In fact, since the polar ring can be a narrow annulus, usually only the extreme value, at the border of the ring, is expected to be reliable.

A final caveat is that the mass of the polar ring itself is dynamically significant (this is obviously an observational bias), and that its introduction in the potential can completely change the conclusions—since in this case, polar rings cannot be considered as test particles tracing the potential, as they considerably modify the potential in their neighborhood, making a comparison of equatorial and polar velocities useless. Sackett & Sparke (1990) demonstrate in particular that for NGC 4650A no dark matter would be required if the total mass of the polar ring would be 4 times the H I gas mass observed. Then, the polar ring system would have a mass comparable to the main galaxy itself—a situation similar to the large ring mass estimated for NGC 660 (Sec. *6.3*).

Kinematical data of three more polar ring galaxies were obtained by Reshetnikov & Combes (1994), who find comparable maximum velocities in the equatorial and polar planes, although they are not measured at the same radii. When the polar ring is well outside the main body, this strongly suggests the existence of a dark halo, though the determination of its flattening is impossible. Mass models give a dark to luminous mass ratio between 1.5 and 3, within 20 kpc. When the polar ring is inside the visible disk, the equality of polar and equatorial velocities occurs because the material of the ring is sensing the potential of the polar disk itself.

This might be the main conclusion of kinematical studies of polar rings: these objects will hardly help to test the three-dimensional shape of the dark halo. The total observed mass (i.e., H I gas, plus the optical component, using $\mathcal{M}/L=4$) is in itself enough to significantly perturb the local potential, and it is likely that the luminosity of polar rings is underestimated due to severe extinction in such edge-on objects (Reshetnikov *et al.* 1994).

6.3 A Mass Model for NGC 660

The situation is in principle better in NGC 660, since the rotation curves of both the disk and polar ring can be deter-

TABLE 4. Mass model parameters.

	Bulge	Disk	Ring	Halo
Mass [a]	1.4	19.4	15.5	21.6 10^9 $M_\odot$
radius r_1 [b]	0.57	1.4	8	9 kpc
radius r_2 [b]	–	–	12 kpc	–
Scalelength h	–	0.32	1 kpc	–

Notes to TABLE 4.

[a] Includes H I and H_2 gas masses; in the I-band a constant M/L ratio of 1.25 was assumed

[b] r_1 and r_2 are the characteristic radii of the Toomre disks

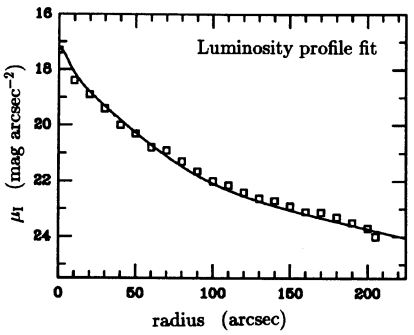

FIG. 20. *I*-band radial luminosity profile of NGC 660 and its polar ring. The solid line is the best fit to the profile, and squares represent the observations, see Fig. 1(e).

mined from emission lines, though the disk Hα rotation curve may be different from the H I and CO curves, which are similar (Fig. 9); the latter has been adopted for our model calculations. In NGC 660 the ring is larger than the disk, like in NGC 4650A, and there is no overlap between the two ranges of radii in which the rotation curves could be measured. A difference with NGC 4650A is the fact that the rotation velocity of the disk in NGC 660 (150 km s^{-1} for the cold gas) is significantly higher than that of the polar ring (125 km s^{-1} on average). A mass model is needed to determine whether dark matter is required to account for the polar ring velocities.

We therefore tried to model the observed properties of the NGC 660 system with a four-component mass model, including a bulge, disk, polar ring, and dark halo. The bulge is represented by a Plummer component, of mass $\mathcal{M}_b$ and size r_b, and the disk by an exponential disk with mass $\mathcal{M}_d$, size r_d, and finite thickness h_d. The dark halo, which could be flattened, has been parametrized as

$$\rho_h(R,z)=\rho_0[1+1/r_h^2(R^2+z^2/q^2)]^{-1}$$

(cf. Sackett & Sparke 1990), where q is the axial ratio of the isodensity curves, which are flattened ellipsoids, ρ_0 is the central density, and r_h the core radius. In the limit of zero flattening, the halo becomes an isothermal sphere and the corresponding rotation curve is asymptotically flat. In order to use well-known analytical density-potential pairs (e.g., Sackett & Sparke 1990), we represent the polar ring distribution by the subtraction of two $n=2$ Toomre disks, with equal central surface density. The characteristic radii of these two Toomre disks, r_1 and r_2, are listed in Table 4.

First we fitted the observed radial luminosity distribution in the *I*-band with three luminous components (Fig. 19), see Table 4 for the best-fit parameters. We then added the gaseous mass and, with a constant $\mathcal{M}/L$ ratio, try to reproduce the observed rotation velocities. Since the potential is nonaxisymmetric in the polar and the equatorial plane (due to the presence of the polar ring), we obtained the equatorial V_{eq} and polar V_{pol} velocities by tabulating the two-dimensional potential in these two planes, and computing the closed orbits by the shooting method.

The results, using only the luminous components, are shown in Fig. 20(a). We adopted the same $\mathcal{M}/L$ ratio, 1.25 in the *I*-band, for all three components. The predicted V_{eq} and V_{pol} are plotted as separate curves. The orbits are significantly elongated within the optical disk only, while in the polar ring itself the potential is practically round. There is undoubtedly need for a dark halo in the outer parts of the polar ring, though the amount of dark matter is not larger than the luminous mass. In fact, we succeed to fit all rotation velocities using a spherical halo, with a total dark-to-luminous mass ratio of 0.6 [see Fig. 21(b)]. This figure would be higher if the dark halo is assumed to be flattened in the direction of the main central disk, but it could be lower as well, if it was flattened in the direction of the polar ring.

The estimated total (stellar+gaseous) present-day mass of the disk is about $2\times10^{10}\mathcal{M}_\odot$, comparable to that of the dark component, while the mass of the accreted polar ring is only a bit less, $1.5\times10^{10}\mathcal{M}_\odot$, and the bulge mass is almost negligible ($0.14\times10^{10}\mathcal{M}_\odot$). Thus, the polar ring is an important mass component in NGC 660, containing about one-quarter of the total mass.

7. CONCLUSIONS

We have presented H I, CO, and Hα line observations and *BVRIJHK'*-band photometry of the polar ring LINER galaxy NGC 660. The gas mass represents nearly 20% of the total luminous mass of the system, and is about equally distributed between the main body and the polar ring, which is unusual. Most polar ring systems are lenticular or early type galaxies, and NGC 660 is at present the only late-type galaxy

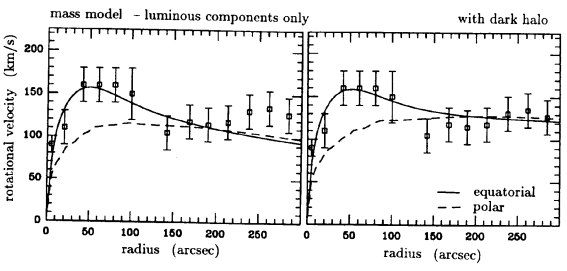

FIG. 21. Results of bulge/disk/polar ring/dark halo mass model fits to the observed rotation curves of the disk and polar ring of NGC 660. The full lines are the computed equatorial (disk) velocities, and the dashed lines the polar velocities. (a) Using luminous components only, and (b) including a spherical dark halo (see the text).

known with such an outer inclined ring. This allowed us to better determine the rotation velocities in the main disk, and to derive an accurate mass model for the system.

Using a deep *I*-band image, and assuming a constant $\mathcal{M}/L$ ratio for the luminous matter, we constructed a mass model including a bulge, exponential disk, and polar ring. The latter contains about one-third of the total luminous mass, which is not sufficient to explain the observed flat or rising rotation curve of the polar ring, which requires an additional dark halo. However, the three-dimensional shape of the halo cannot be constrained, since the equatorial and polar velocities are not known at the same radii. If spherical, the dark halo has a mass of 60% of the total luminous matter inside the outermost radius of the polar ring. The polar ring is quite massive, representing about 25% of the total mass, allowing it to stabilize itself through self-gravity.

We wish to thank Dr. J. S. Young, Dr. M. Capaccioli and Dr. P. Benvenuti for making their optical images available to us, A. Coolen for his help with the preparation of the Westerbork maps, Dr. F. Viallefond for his support with the Meudon GIPSY system, Dr. Y. K. Ng for digitizing a Palomar Sky Survey plate, and Luca van Driel for her help in preparing the illustrations. W.v.D. wishes to thank the Observatoire de Paris-Meudon for their kind support during his visits. This paper is based partially on observations collected at the European Southern Observatory, La Silla, Chile. IRAF is distributed by the National Optical Astronomy Observatories, which is operated by the Association of Universities for Research in Astronomy, Inc. (AURA) under cooperative agreement with the National Science Foundation. We have made use of the NASA/IPAC Extragalactic Database (NED) which is operated by the Jet Propulsion Laboratory, California Institute of Technology, under contract with the National Aeronautics and Space Administration. The Westerbork Radio Observatory is operated by the Netherlands Foundation for Research in Astronomy (NFRA/ASTRON) with financial support from the Netherlands Organization for the Advancement of Research (NWO).

REFERENCES

Aalto, S., Black, J. H., Johanson, L. E. B., & Booth, R. S. 1991, A&A, 249, 323
Allen, R. J., Ekers, R. D., & Terlouw, J. P. 1985, in Data Analysis in Astronomy, edited by V. di Gesu *et al.* (Plenum, New York), p. 271
Arimoto, N., & Bica, E. 1989, A&A, 222, 89
Arimoto, N., & Yoshii, Y. 1986, A&A, 164, 260
Armus, L., Heckman, T. M., & Miley, G. K. 1989, ApJ, 347, 727
Arnaboldi, M., & Galletta, G. 1993, A&A, 268, 411
Baan, W. A., Gusten, R., & Haschick, A. D. 1986, ApJ, 305, 830
Baan, W. A., Haschick, A. D., & Henkel, C. 1989, ApJ, 346, 680
Baan, W. A., Haschick, A. D., & Uglesich, R. 1993, ApJ, 415, 140
Baan, W. A., Rhoads, J., & Haschick, A. D. 1992, ApJ, 401, 508
Begeman, K. 1989, A&A, 223, 47
Benvenuti, P., Capaccioli, M., & D'Odorico, S. 1976, A&A, 53, 141
Bosma, A. 1981, AJ, 86, 1791
Braine, J., & Combes, F. 1992, A&A, 264, 433
Braine, J., *et al.* 1993, A&AS, 97, 887
Briggs, F. H., Wolfe, A. M., Krumm, N., & Salpeter, E. E. 1980, ApJ, 238, 510
Casoli, F., Viallefond, F., Combes, F., & Boulanger, F. 1990, A&A, 233, 357
Casoli, F., *et al.* 1992, A&A, 264, 55
Chini, R., Kreysa, E., Krugel, E., & Mezger, P. G. 1986, A&A, 166, L8
Claussen, M. J., & Lo, K. Y. 1986, ApJ, 308, 592
Cohen, M. 1992, AJ, 103, 1734
Combes, F. 1988, in Galactic and Extragalactic Star Formation, edited by R. E. Pudritz and M. Fich (Kluwer, Dordrecht), p. 475
Combes, F. 1994, in The Formation of Galaxies, Fifth Canary Islands Winter School, edited by C. Muñoz-Tuñon (in press)
Combes, F., Braine, J., Casoli, F., Gerin, M., & van Driel, W. 1992, A&A, 259, L65 (Paper I)
Combes, F., & Gerin, M. 1985, A&A, 150, 327
Condon, J. J. 1980, ApJ, 242, 894
Condon, J. J. 1983, ApJS, 53, 459
Condon, J. J. 1987, ApJS, 65, 485
Condon, J. J., & Broderick, J. J. 1988, AJ, 96, 30
Condon, J. J., Condon, M. A., Gisler, G., & Puschell, J. J. 1982, ApJ, 252, 102
Condon, J. J., *et al.* 1990, ApJS, 73, 359
de Jong, T., & Brink, K. 1987, in Star Formation in Galaxies, edited by C. J. Lonsdale Persson, NASA Conf. Publ. No. 2466, p. 323
de Vaucouleurs, G., de Vaucouleurs, A., & Corwin, G. 1976, Second Reference Catalogue of Bright Galaxies (University of Texas Press, Austin) (RC2)
de Vaucouleurs, G., de Vaucouleurs, A., Corwin, G., Paturel, G., & Fouqué, P. 1991, Third Reference Catalogue of Bright Galaxies (Springer, Berlin) (RC3)
Dressel, L. L., & Condon, J. J. 1978, ApJS, 36, 53
Dubinski, J., & Christodoulou, M. 1994, ApJ, 424, 615
Filippenko, A. V. 1989, in Active Galactic Nuclei, IAU Symposium No. 134, edited by D. E. Osterbrock and J. S. Miller (Kluwer, Dordrecht), p. 495
Fukugita, M., *et al.* 1991, ApJ, 376, 8
Fullmer, L., & Lonsdale, C. 1988, Cataloged Galaxies and Quasars Observed in the *IRAS* Survey—Version 2 (Jet Propulsion Laboratory, Pasadena)
Garcia, A. M. 1993, A&AS, 100, 47
Garwood, R. W., Helou, G., & Dickey, J. M. 1987, ApJ, 322, 88
Geller, M. J., & Huchra, J. P. 1983, ApJS, 52, 61
Gerin, M., Nakai, N., & Combes, F. 1988, A&A, 203, 44
Gillet, F. C., *et al.* 1988, AJ, 96, 116
Giovanardi, C., & Salpeter, E. E. 1985, ApJS, 58, 623
Gottesman, S. T., & Mahon, M. E. 1989, in Paired and Interacting Galaxies, IAU Colloquium No. 124, edited by J. W. Sulentic, W. C. Keel, and C. M. Telesco, NASA Conf. Publ. No. 3098, p. 209
Hamabe, M., & Ichikawa, T. 1992, in Astronomical Data Analysis and Software I, edited by D. M. Worall and C. Beimesderfer (ASP Conference Series, San Francisco), Vol. 25, p. 325
Heckman, T. M. 1987, in Observational Evidence of Activity in Galaxies, IAU Symposium No. 121, edited by E. Ye. Khachikhian, K. J. Fricke, and J. Melnich (Reidel, Dordrecht), p. 421
Heckman, T. M., van Breugel, W., Miley, G. K., & Butcher, H. R. 1983, AJ, 88, 1077
Helou, G., Kahn, I. R., Malek, L., & Boehmer, L. 1989, ApJS, 68, 151
Henkel, C., Wouterloot, J. G. A., & Bally, J. 1986, A&A, 155, 193
Hodge, P. W. 1966, Atlas and Catalog of H II regions (University of Washington, Seattle)
Hodge, P. W. 1982, AJ, 87, 1341
Högbom, J. A. 1974, A&AS, 15, 417
Huchtmeier, W. K. 1982, A&A, 110, 121
Huchtmeier, W. K., & Richter, O.-G. 1988, A&A, 203, 237
Huchtmeier, W. K., & Richter, O.-G. 1989, A General Catalog of H I Observations of Galaxies (Springer, Berlin)
Hummel, E. 1980, A&AS, 41, 151

Hummel, E. 1981, A&A, 93, 93
Hummel, E., van der Hulst, J. M., & Dickey, J. 1984, A&A, 134, 207
Hummel, E., van der Hulst, J. M., Keel, W. C., & Kennicutt, R. C. 1987, A&AS, 70, 517
Ichikawa, T., & Hamabe, M. 1992, in Astronomical Data Analysis and Software I, edited by D. M. Worall and C. Beimesderfer (ASP Conf. Ser., San Francisco), Vol. 25, p. 322
Ichikawa, T., Tarusawa, K., Yanagisawa, K., Itoh, N., & Ueno, M. 1994, in Astronomy from Wide Field Imaging, IAU Symposium No. 161 (in press)
Israel, F. P., & van der Hulst, J. M. 1983, AJ, 88, 1736
Jones, D. L., Sramek, R. A., & Terzian, Y. 1981, ApJ, 246, 28
Katz, N., & Richstone, D. O. 1984, AJ, 89, 975
Keel, W. C. 1983a, ApJS, 52, 229
Keel, W. C. 1983b, ApJ, 269, 466
Keel, W. C. 1984, ApJ, 282, 75
Kennicutt, R. C., & Pogge, R. W. 1990, AJ, 99, 61
Kobayashi, Y., *et al.* 1994, in Infrared Astronomy with Arrays: The Next Generation, edited by I. S. McLean, Exp. Astronomy, 3, 135
Kodama, T., & Arimoto, N. 1994, A&A, in preparation
Landolt, A. U. 1992, AJ, 104, 340
Lu, N. Y., *et al.* 1993, ApJS, 88, 383
Morgan, C. G., & Hartwick, F. D. A. 1988, ApJ, 328, 381
Nilson, P. 1973, Upsala General Catalogue of Galaxies, Upsala Astron. Ann. 6 (UGC)
Paturel, G., Bottinelli, L., Gouguenheim, L., & Fouqué, P. 1990, Catalogue of H I-Data (Observatories of Lyon and Paris-Meudon, France)
Reshetnikov, V. P., & Combes, F. 1994, A&A, 291, 57
Reshetnikov, V. P., Hagen-Thorn, V. A., & Yakovleva, V. A. 1994, A&A, 290, 693
Rice, W., *et al.* 1988, ApJS, 68, 91
Richter, O.-G., Sackett, P. D., & Sparke, L. S. 1994, AJ, 107, 99
Rickard, L. J., *et al.* 1982, ApJ, 252, 147
Rickard, L. J., & Harvey, P. M. 1984, AJ, 89, 1520
Roche, P. F., Aitken, D. K., Smith, C. H., & Ward, M. J. 1991, MNRAS, 248, 606
Rots, A. H. 1980, A&AS, 41, 189
Rowan-Robinson, M., & Crawford, J. 1989, MNRAS, 238, 523
Rubin, V. C., Burstein, D., Ford, W. K., & Thonnard, N. 1985, ApJ, 289, 81
Sackett, P. D., & Sparke, L. S. 1990, ApJ, 361, 408
Sanders, D. B., & Mirabel, I. F. 1985, ApJ, 298, L31
Sanders, D. B., Solomon, P. M., & Scoville, N. Z. 1984, ApJ, 276, 182
Schechter, P., Sancisi, R., van Woerden, H., & Lynds, C. R. 1984, MNRAS, 208, 111
Schweizer, F., Whitmore, B. C., & Rubin, V. C. 1983, AJ, 88, 909
Shaw, M. 1993, MNRAS, 261, 718
Soifer, B. T., Boehmer, L., Neugebauer, G., & Sanders, D. B. 1989, AJ, 98, 766
Sparke, L. S. 1986, MNRAS, 219, 657
Spitzer, L. 1978, Physical Processes in the Interstellar Medium (Wiley, San Fransisco)
Tully, R. B. 1987, Catalog of Nearby Galaxies (Cambridge University Press, Cambridge)
van der Hulst, J. M., *et al.* 1992, in Astronomical Data Analysis and Software I, edited by D. M. Worall and C. Beimesderfer (ASP Conference Series, San Fransico), Vol. 25, p. 131
van Driel, W. 1995, in Stellar Populations, IAU Colloquium No. 164, edited by G. Gilmore and P. C. van der Kruit (in press)
van Driel, W., Combes, F., Nakai, N., & Yoshida, S. 1994, in Astronomy with Millimeter and Submillimeter Wave Interferometry, IAU Colloquium No. 140, edited by M. Ishiguro and J. Welch (ASP Conf. Ser., San Francisco), Vol. 59, p. 347
van Driel, W., de Graauw, Th., de Jong, T., & Wesselius, P. R. 1993, A&AS, 101, 207
van Driel, W., van Woerden, H., & Balkowski, C. 1989, A&A, 218, 49
van Driel, W., & van den Broek, A. C. 1991, A&A, 251, 431
van Driel, W., & van Woerden, H. 1991, A&A, 241, 71
van Gorkom, J. H., Schechter, P. L., & Kristian, J. 1987, ApJ, 314, 457
Veilleux, S., & Osterbrock, D. E. 1987, ApJS, 63, 295
Vennik, J. 1984, Tartu Astroph. Obs. Teated, 73, 3
Vennik, J. 1986, ANac, 307, 157
Véron-Cetty, M. P., & Véron, P. 1993, A Catalogue of Quasars and Active Nuclei, 6th Edition, ESO Sci. Report No. 13
Wakamatsu, K. 1993, AJ, 105, 1745
Warner, P. J., Wright, M. C. H., & Baldwin, J. E. 1973, MNRAS, 63, 163
Werner, M. W., Bushouse, H. A., Telesco, C. M., & Decher, R. 1986, BAAS, 18, 1021
Whitmore, B. C., McElroy, B. D., & Schweizer, F. 1987, ApJ, 314, 439
Yanagisawa, K., Itoh, N., Ichikawa, T., Tarusawa, K., & Ueno, M. 1994, in Astronomy from Wide Field Imaging, IAU Symposium No. 161 (in press)
Yoshida, S., *et al.* 1994, in Future Utilization of Schmidt Telescopes, IAU Colloqium No. 148, edited by R. D. Cannon and B. Hidayat (ASP Conf. Ser., San Francisco) (in press)
Young, J. S., Kleinmann, S. G., & Allen, L. E. 1988, ApJ, 334, L63
Young, J. S., Schloerb, F. P., Kenney, J. D., & Lord, S. D. 1986, ApJ, 304, 443
Young, J. S., & Scoville, N. Z. 1991, ARA&A, 29, 581

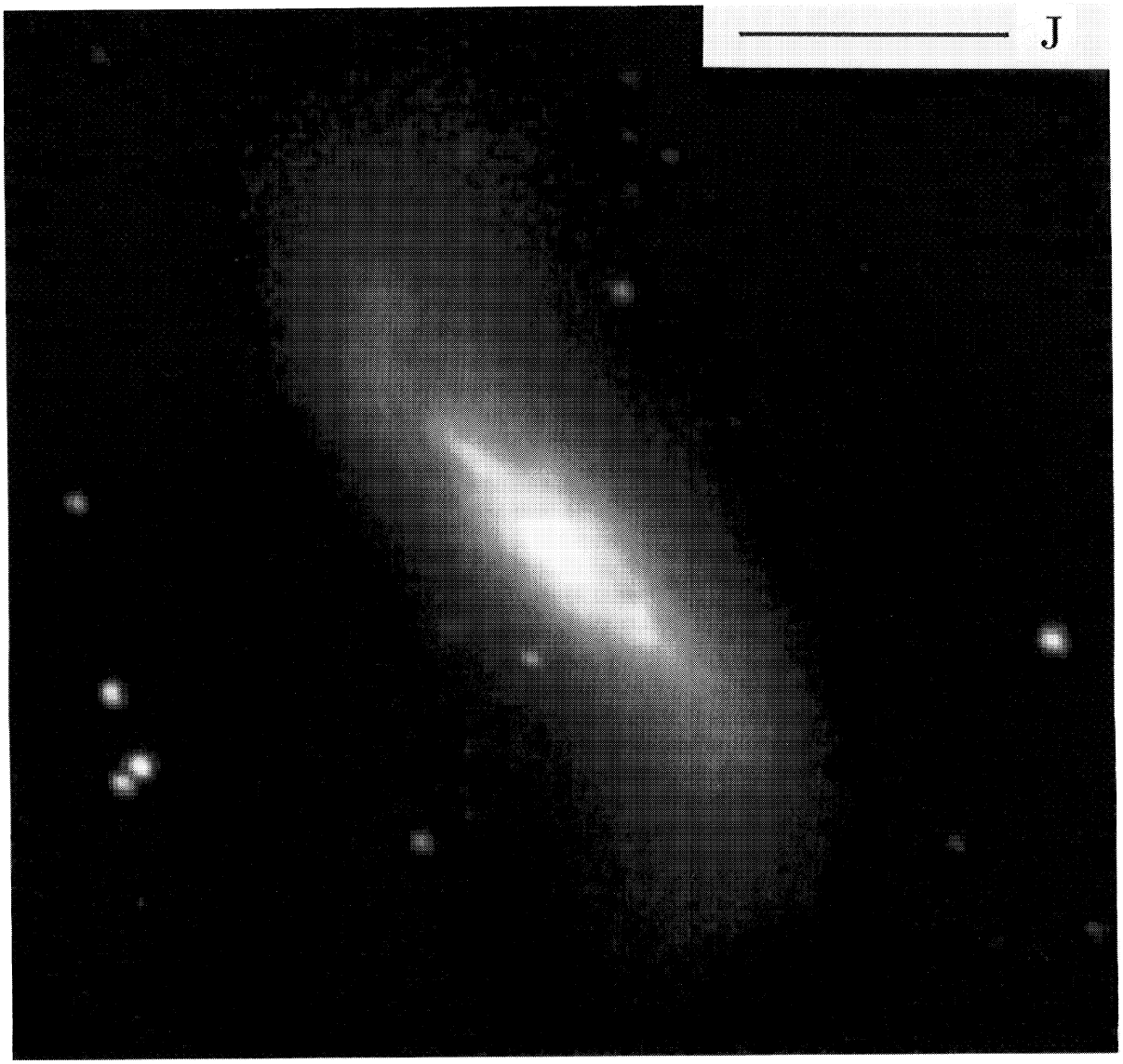

(a)

FIG. 3. Near-infrared images obtained with the PICNIC system, image size is 4.'2×4.'2, except for (d). The bar indicates a scale of 1′. (a) J-band image, greyscale steps (dark to light) are from 21.5 to 16 mag arcsec^{-2}, (b) K'-band image, greyscale steps (dark to light) from 21.25 to 15 mag arcsec^{-2}, (c) unsharp masked K'-band image (see text), and (d) $J-K'$ color map, greyscale steps (dark to light) from 1.1 to 1.9 mag.

van Driel *et al.* (see page 947)

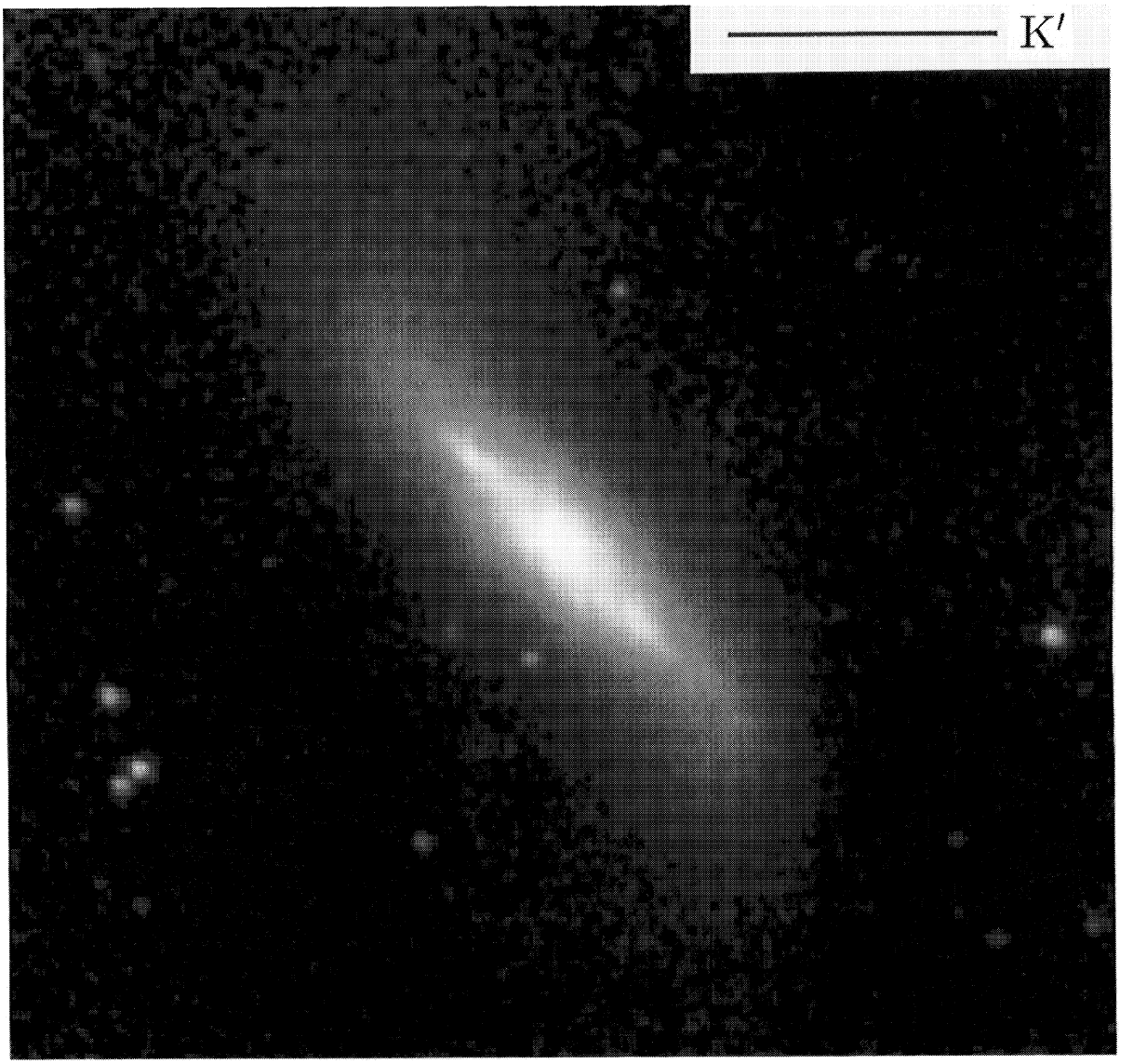

(b)

FIG. 3. (continued)

Van Driel *et al.* (see page 947)

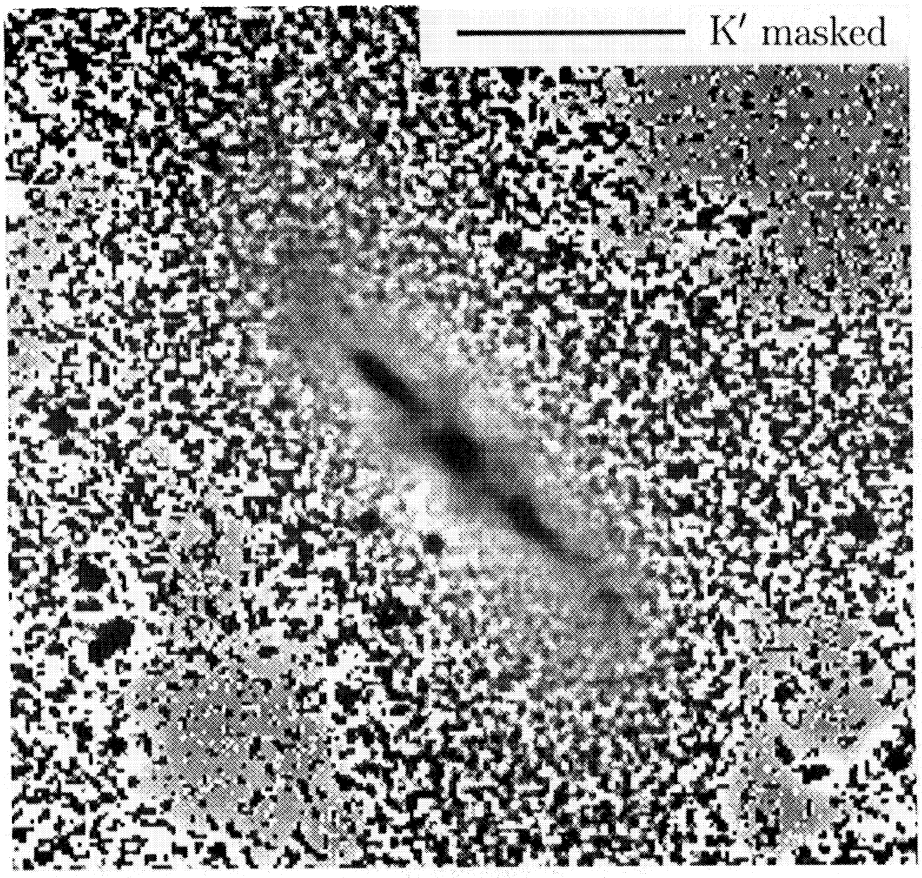

(c)

FIG. 3. (continued)

Van Driel *et al.* (see page 947)